Geochimica et Cosmochimica Acta 361 (2023) 245–264

Contents lists available at ScienceDirect

Geochimica et Cosmochimica Acta

journal homepage: www.elsevier.com/locate/gca

The mineralogy and alteration history of the Yamato-type (CY) carbonaceous chondrites

M.D. Suttle [a,b,*], A.J. King [b], C.S. Harrison [b], Q.H.S. Chan [a,c], A. Greshake [d], R. Bartoschewitz [e], A.G. Tomkins [f], T. Salge [g], P.F. Schofield [b], S.S. Russell [b]

[a] School of Physical Sciences, The Open University, Walton Hall, Milton Keynes MK7 6AA, UK
[b] Planetary Materials Group, Natural History Museum, Cromwell Road, London SW7 5BD, UK
[c] Department of Earth Sciences, Royal Holloway, University of London, Egham, Surrey TW20 0EX, UK
[d] Museum für Naturkunde, Leibniz-Institut für Evolutions und Biodiversitätsforschung, Invalidenstraße 43, 10115 Berlin, Germany
[e] Bartoschewitz Meteorite Laboratory, Weiland 37, D-38518 Gifhorn, Germany
[f] School of Earth, Atmosphere and Environment, Melbourne, Victoria, Australia
[g] Imaging and Analysis Centre, Natural History Museum, Cromwell Road, London SW7 5BD, UK

ARTICLE INFO

Associate editor: Yves Marrocchi

Keywords:
Carbonaceous chondrites
C-type asteroids
CY chondrites
Aqueous alteration
Thermal metamorphism

ABSTRACT

The CY chondrites are a group of thermally metamorphosed carbonaceous chondrites. Although they share similarities with the CM and CI chondrites, their primary properties argue for a distinct classification. Previous studies have highlighted their isotopically heavy bulk compositions ($\delta^{17}O = 10$ ‰, $\delta^{18}O = 21$ ‰, $\Delta^{17}O = 0$ ‰) and exceptionally high sulphide abundances (10–30 vol%). In this work we explore their petrography and alteration history. The CYs accreted low abundances of chondrules (15–20 area%) with average apparent diameters slightly larger (~320–340 μm) than the CM chondrites. In contrast to the CMs, the CYs record an early episode of brecciation prior to the main window of aqueous alteration. Subsequent fluid activity produced a range of alteration extents with both CY2 and CY1 chondrites documented. Phyllosilicate minerals in the CYs were a mix of serpentine and saponite (including occurrences of Na-saponite) with minor quantities of chlorite (within chondrules). An initial generation of Fe-sulphides formed by sulfidation of metal, and by precipitation from S-rich fluids. Three generations of carbonates are recognized, an early generation that infilled voids left by brecciation and co-precipitated with sulphide, a later generation that co-precipitated with magnetite and a final Fe-Mg-bearing generation which formed large (>100 μm) clasts. Only the first-generation carbonates are found in the CY2s, while the CY1s preserve all three generations. Phosphates occur as Ca-apatite or rarely as Mg-bearing apatite and have hydroxylapatite compositions, indicating low halogen activities in the alteration fluids. Refractory oxides (ilmenite and Cr-spinel) occur as precipitates adhering to the margins of phyllosilicates. They formed late in the alteration sequence and attest to oxidizing conditions. During the late-stages of aqueous alteration Fe-sulphides were replaced by magnetite. Thermal metamorphism (Stage II-IV: ~300–750 °C) overprinted aqueous alteration leading to dehydration and recrystallization of the phyllosilicate matrix and the decomposition of some carbonate phases. Most Fe-sulphide grains survived heating without decomposition as initial partial decomposition from pyrrhotite to troilite under closed system conditions led to elevated fS_2 gas and resulted in a stabilizing effect. Retrograde reactions between trapped S_2 gas and metal/magnetite formed a final generation of Fe-sulphides. The survival of Fe-sulphides and their stochiometric troilite compositions are evidence for near-closed system heating. Analysis of organic matter by Raman spectroscopy supports an interpretation of short-duration heating (on the scale of minutes to days), at peak temperatures between 750 and 900 °C. Thus, an impact event was the most likely cause of metamorphic heating.

* Corresponding author at: School of Physical Sciences, The Open University, Walton Hall, Milton Keynes MK7 6AA, UK.
E-mail addresses: martin.suttle@open.ac.uk (M.D. Suttle), a.king@nhm.ac.uk (A.J. King), c.harrison@nhm.ac.uk (C.S. Harrison), queenie.chan@rhul.ac.uk (Q.H.S. Chan), ansgar.greshake@mfn-berlin.de (A. Greshake), meteorite-lab@t-online.de (R. Bartoschewitz), andy.tomkins@monash.edu (A.G. Tomkins), t.salge@nhm.ac.uk (T. Salge), p.schofield@nhm.ac.uk (P.F. Schofield), sara.russell@nhm.ac.uk (S.S. Russell).

https://doi.org/10.1016/j.gca.2023.09.024
Received 10 July 2023; Accepted 28 September 2023
Available online 30 September 2023

1. Introduction

Chondrites are a large and diverse set of primitive, undifferentiated meteorites united by the presence of chondrules; spherical particles with igneous textures, embedded within a matrix of fine-grained, volatile-rich material (Scott and Krot, 2003; Weisberg et al., 2006). Chondrites are relicts of the early Solar System representing precursor materials to (Chambers, 2004; Alexander, 2005) and/or by-products of planetary formation (Krot et al., 2005; Kleine et al., 2005). The carbonaceous chondrites are primitive and undifferentiated meteorites that appear to have formed in the outer regions of the early Solar System, most likely beyond the orbit of Jupiter (Warren, 2011; Kleine et al., 2020) and/or close to the protosolar water–ice "snowline" (Lipschutz et al., 1999; Krot et al., 2015). They have chemical compositions that closely match the composition of the Sun (Kallemeyn and Wasson, 1981) and most have high organic compound (Kerridge, 1985; Alexander et al., 2012, 2013; Kebukawa et al., 2017) and water contents (Vacher et al., 2020; Bates et al., 2023). Carbonaceous chondrites are also associated with primitive C-type asteroids (Feierberg et al., 1985; Beck et al., 2018), which are a principal focus of several recent space missions (e.g., Hayabusa-2, OSIRIS-REx and Dawn).

The CY ("Yamato-type") chondrites are a newly proposed group of carbonaceous chondrites (Bischoff and Metzler, 1991; Ikeda, 1992; King et al., 2019; Suttle et al., 2021a). They are a small class composed of six Antarctic meteorites (B-7904, Y-86720, Y-82162, Y-86029, Y-86789, Y-980115) recovered from the Yamato Mountains in East Antarctica (King et al., 2019), and three hot desert meteorites (Dho 225, Dho 735 and Dho 1988) recovered from Oman (Ivanova et al., 2010; Suttle et al., 2021a). Additional unstudied meteorites which could be members of the CY group, based upon the O-isotope compositions and petrographic descriptions given in the Meteoritical Bulletin, include Dho 2046 (Bouvier et al., 2017a), Dho 2066 (Gattacceca et al., 2019) and NWA 4757 (Connolly et al., 2008).

The petrography of the CYs records an extended period of aqueous alteration resulting in near-complete replacement of their primary texture with hydrated secondary phases (phyllosilicates, tochilinite, carbonates and magnetite) (Akai, 1990; Tomeoka et al., 1989; Tomeoka, 1990; Ikeda, 1992; Tonui et al., 2002; King et al., 2019; Suttle et al., 2021a). As with other hydrated chondrite groups, the CY chondrites span a range of aqueous alteration extents. Three of the CYs (Y-82162, Y86029 and Y-980115) lack chondrules and calcium-aluminium-rich inclusions (CAIs) and have historically been classified as CI or CI-like chondrites (King et al., 2015a, 2015b). A CY1 classification has been proposed (King et al., 2019; Bates et al., 2021). Conversely, the remaining CYs all contain aqueously altered chondrules and are considered CY2 chondrites (King et al., 2019; Bates et al., 2021; Suttle et al., 2021a). From this point forwards, we employ the term "CY" to encompass the entire group and use "CY1s" or "CY2s" to denote a subset of the population affected by a specific alteration extent.

The CY meteorites were affected by short-duration post hydration thermal metamorphism, possibly caused by an impact event or solar radiation, as inferred from the rapid heating implied from Fe-Mg zoning profiles in primary mafic silicates within the CY2 B-7904 (10–1000 days at temperatures of <700 °C (or between 1 and 100 h at 890 °C), Nakato et al., 2008) and the depleted noble gas budget of the CY1 Y-980115 (>500 °C for <100 min, Kikuchi et al., 2015). The entire CY group have low to moderate water contents (~2–8 wt%, Lipschutz et al., 1999; King et al., 2015b; Vacher et al., 2020) and matrices dominated by dehydroxylated former phyllosilicates intermixed with microcrystalline secondary olivine. Metamorphic temperatures are estimated between 500 and 900 °C (Akai, 1992; Matsuoka et al., 1996; Nakamura, 2005; Nakato et al., 2008; King et al., 2015a; Suttle et al., 2021a).

In this study, we provide the first detailed petrographic analysis of the wider CY group (six meteorites: B-7904, Dho 1988, Y-82162, Y-86029, Y-86720, and Y-86789) with the aim of defining their accretionary properties and deciphering alteration history.

2. Methods

2.1. Samples

Meteorites were acquired by non-destructive research loan from National Institute of Polar Research (NIPR), Japan and the Museum für Naturkunde (MfN), Berlin (Table 1). In this study we investigated six meteorites, five are Antarctic specimens recovered from the Yamato mountains in East Antarctica and the remaining meteorite (Dho 1988) is a hot desert sample recovered from the Dhofar region in Oman and previously described in Suttle et al. (2021a). The combined surface area of the meteorite thin sections investigated in this work is 393 mm^2. The smallest meteorite section (Y-86029) has an exposed area of 23.7 mm^2, whereas the largest (B-7904) has an area of 99.0 mm^2.

Each sample was analysed petrographically at the Natural History Museum (NHM), London under scanning electron microscope (SEM) using a Zeiss EVO LS15 fitted with an Oxford Instruments' 80 mm^2 X-Max silicon drift detector energy dispersive spectrometer. We collected backscatter electron (BSE) images, quantitative standards-based energy dispersive X-ray spectrometry (EDS) point spectra and high-spatial resolution elemental X-ray maps.

2.2. SEM and elemental analysis

Whole-section EDS maps were produced by montaging multiple individual fields, each composed of 256 × 192 pixels (555 μm × 415 μm, approximately 0.23 mm^2, with a pixel size of ~1.9 μm). Maps were collected at 20 kV, with a 1.5 nA beam current resulting in high output count rates (>50 kcps). Each field had a total acquisition time of approximately 270 s. Composite elemental maps for each section are given in the supplementary material. Maps were used to explore intra sample variability, coarse-scale texture, and the distribution of phases. Chondrules and CAIs were identified manually from map data and their apparent diameters measured using the ImageJ software (Schindelin et al., 2012) extracting Feret diameters (maximum and minimum lengths) for each object.

Quantitative elemental data were obtained either by standards-based EDS or by wavelength dispersive spectrometry (WDS), depending on the phase under investigation. Silicates, oxides, and metals were analyzed by EDS. Analyses were performed at high vacuum, with an accelerating voltage of 20 kV, a beam current of 1.5 nA and a fixed optimal working distance (10 mm). Output count rates were typically between 40 and 60 kcps for silicate minerals. Spot analyses were acquired with a 5 s acquisition time and ~30 % deadtime. The system's beam current was monitored regularly using a built-in Faraday cup. We calibrated the EDS system (for peak position and intensity) using our internal cobalt metal reference sample. Data were processed using the Oxford Instruments AZtec software (version 5.0 SP1) applying standard XPP matrix correction routines (Pouchou and Pichoir, 1991). For silicates and oxides, weight totals (wt.%) were determined using the "*oxygen by stoichiometry*" quantification routine and metals were calculated using the "*all elements*" routine. The accuracy and precision for major rock-forming silicate cations were cross-checked against analyses on the Smithsonian reference sample augite NMNH 122142 (Kakanui, New Zealand), the composition of which is known from dissolution. Detection limits are on the order of 0.1–0.3 wt%, and analytical uncertainties have a relative error dependent on the element's concentration. Major elements (>10 wt%) have uncertainties of 1–3 %, minor elements (1–10 wt%) have uncertainties of ~10 % and trace elements (<1 wt%) have uncertainties between 30 and 50 %.

Sulphides and the fine-grained matrix were analyzed by WDS using a Cameca SX100 electron microprobe, equipped with 5 WD spectrometers. Analyses were performed using a 20 kV accelerating voltage and 20 nA beam current. Sulphides were investigated using a small spot size (4 μm), and matrix analyses used a "broad beam" approach (~10 × 10 μm region) (e.g., Lauretta et al., 2001). This approach violates a key

Table 1
List of meteorite sections studied in this work and data extracted from BSE maps. Note: Roman numerals given under the "proposed classification" heading reflect the heating stage, using the scheme of Nakamura (2005).

Meteorite	Source	Sample ID	Section surface area (mm2)	Texture	Chondrule abundance (N=?)	Chondrule abundance (area %)	Chondrule size, avg. (μm)	CAI abundance (area%)	Proposed classification
Y-86029	NIPR	51-A	23.7	Brecciated	*No apparent chondrules.*			≪1.0	CY1, H:III
Y-82162	NIPR	45–1	38.1	Minor brecciation	*No apparent chondrules.*			≪1.0	CY1, H:III
B-7904	NIPR	64-A	99.0	No apparent brecciation	189	18.4	320	<1.0	CY2, H:IV
Y-86720	NIPR	59-A	82.4	No apparent brecciation	110	9.6	310	<0.5	CY2, H:IV
Y-86789	NIPR	81-A	85.0	No apparent brecciation	59	7.1	360	N/A.	CY2, H:IV
Dho 1988	MfN	MNB-XV-II-36	65.0	Brecciated	38	15.2	530	9.8	CY2, H:III/IV
Total			***393.2***	***Average***		***12.6***	***340***		

assumption of the matrix correction routine (a homogenous interaction volume). Under these conditions the matrix correction is likely to generate high totals (Llovet et al., 2021). Despite these limitations broad beam techniques are frequently used as a means of obtaining an approximate chemical composition from the mixed phase, fine-grained matrix in chondritic meteorites which are otherwise difficult to obtain compositional data from. Prior to analysis, the system was calibrated using a suite of mineral references, specific to each element investigated. Oxygen was calculated by stoichiometry. After analysis, the in-house Cameca PAP matrix correction software was used to remove artefacts arising from atomic number, absorption and secondary fluorescence (ZAF) effects. Elemental detection limits for this instrument are on the order of 0.02–0.05 wt%.

Carbonates were analysed by EDS under the same beam conditions as the silicates, oxides and metal (20 kV, 1.5 nA). We employed a "carbon by difference" quantification routine which performs direct quantification of the O-K line and infers the abundance of C assuming an idealized 100% weight total. Analysis of beam sensitive carbonates under these conditions is suboptimal but sufficient to determine approximate major element cation composition (Ca, Mg, Fe and Mn abundance). We used these data to discriminate different carbonate species (e.g., calcite, dolomite, magnesite and siderite) (Fig. S12).

2.3. Raman spectroscopy

Raman spectroscopic analysis was used to analyse the polished surfaces of the meteorite thin sections using a Jobin-Yvon Horiba LabRam HR (800 mm) Raman microprobe located at The Open University (OU). The six CY chondrites were analysed alongside other meteorites, including CI1 Ivuna, CM2 Mighei, CR2 Al Rais, CV3 Allende, and LL3 Huacachina. These non-CY chondrites were analysed to provide a reference to the peak metamorphic temperature experienced by the CY members and allow comparisons between our data with that presented in previous studies (e.g., Chan et al., 2017, 2019a, 2019b). Mechanical polishing artifacts have been previously reported to influence Raman spectra due to the disruption of the soft, opaque carbonaceous phases, of which only the uppermost layer (<1 μm) of the thin section disrupted by mechanical polishing can be excited by the laser (Fries and Steele, 2011). The difference manifested by mechanical polishing is present, though minor, as reflected by the variations between the Raman spectral data of the Allende meteorite thin section and its insoluble organic matter prepared by the demineralization of the bulk meteorite with CsF-HF dissolution (i.e., IOM/acid residue) according to the methods described in Cody and Alexander (2005).

The excitation source was a 514.5 nm (green) laser. Between 12 and 24 spectra were acquired for each sample studied (except Y-82162 from which 315 spectra in total were acquired) in the spectral region 800–2,200 cm^{-1}, which includes the first (~1,000–1,800 cm^{-1}) Raman bands of carbon. The analytical areas were selected to avoid chondrules (i.e., data were collected from the sample matrix), and only the interior of the meteorites was analysed. The slit width and the confocal pinhole aperture were set at 150 μm and 300 μm, respectively, and a 600 grooves mm^{-1} grating was used to disperse the Raman signal, leading to a spectral resolution of approximately 3 cm^{-1}. The laser beam was focused through a microscope equipped with a 100× objective lens (numerical aperture = 0.75). At this magnification and for the laser used, the spot size of the Raman probe was ~1 μm, and the laser power at the sample surface was ~50 μW. The exposure time for each spectrum was 20 s and three accumulations were obtained for each analytical spot to identify and discard spurious signals, such as those from cosmic rays, leading to a total acquisition time of up to 180 s. Peak position was calibrated daily against a silicon wafer prior to sample analyses and no significant shift was observed. Laser power was also checked daily prior to analyses to ensure that the laser power was consistent amongst all samples. The sample surface was re-examined by the optical microscope to check for any damage, and we confirm that no sign of physical damage was observed. Spectral peak identification and methods used in the present study were the same as outlined in the literature (Chan et al., 2019a, 2019b). The peak position (ω) and full width half-maximum (FWHM, Γ) of each Raman band were determined by simultaneous peak fitting to the two-peak Lorentzian and Breit–Wigner–Fano (LBWF) model (Ferrari and Robertson, 2000) and linear baseline correction. Details of the Raman peak fitting procedures and rationales are given in the literature (Chan et al., 2017, 2019a, 2019b). Raman band parameters for each sample were reported as the average of all selected spectra and the uncertainties are the 1σ standard error of the mean of all used spectra. Only fitted data with R^2 values >0.9 are shown in this study.

3. Results

3.1. Brecciation

Three (Y-86029 (CY1), Y-82162 (CY1) and Dho 1988 (CY2)) of the six CY meteorites show evidence of brecciation (Table 1, Figs. S1–S6). Dho 1988 contains a pronounced clastic texture with lithic fragments separated by fractures (Fig. S6). They are infilled by a mixed assemblage of carbonate, sulphide and thermally decomposed phyllosilicate minerals forming veins (previously described in Suttle et al. (2021a)). Mineralized veins are not present in the other CYs, however both the CY1s (Y-86029 and Y-82162) have subtle brecciation textures. In Y-86029, the boundaries between clasts are easily resolvable, being marked by relatively sharp compositional changes (changes in Z value in BSE images). These boundaries are variably accompanied by thin open fractures. Despite the small surface area exposed in the Y-86029 section,

at least ten approximately millimetre-sized clasts can be identified. They have brighter appearances (higher Z value in BSE images, reflecting Fe-enriched compositions) relative to the host matrix. The most prominent clast (found in the upper left corner of the section (Fig. S1)) preserves angular margins. In contrast, many of the other clasts in Y-86029 have rounded edges and transitional boundaries. The matrix in Y-82162 (Fig. S2) has a relatively homogenous appearance with no sharp boundaries between lithologies. However, several subtle outlines reflecting the boundaries of former clasts can be discerned. Relative to Y-86029, Y-82162 has fewer clasts and all of these are small, rounded fragments. Among the remaining three CY sections, (all CY2s: B-7904, Y-86720 and Y-86789) evidence for brecciation is absent.

3.2. Chondrules and CAIs

Chondrules (Fig. 1) are preserved only in the CY2s. Most chondrules are readily distinguishable from the host fine-grained matrix. They typically have dark cores in BSE images and rounded or irregular shapes. Their margins are mantled by thin continuous fine-grained rims (FGRs) and may also be decorated by a locally high abundance of sulphides, forming "armored chondrules" (Bischoff et al., 1993; Marrocchi and Libourel, 2013). Many of the smaller chondrules are, however, less sharply defined, having indistinct boundaries, and lacking clear FGRs (Fig. 1C). These textures are the result of advanced aqueous alteration that progressively replaced anhydrous silicates with phyllosilicates.

In general, chondrules in CY2s are heavily altered, having experienced >50 % (and often close to 100 %) replacement of their primary mineralogy. Several chondrules have coarse fibrous textures reflecting the existence of former phyllosilicates, since dehydrated and/or recrystallized to form secondary olivine (Fig. 1A and B). In addition, Fe-enriched phyllosilicates (and former phyllosilicates) with rounded and nodular textures are present in some chondrules (Fig. 1A and B). They typically have a discontinuous rim of micron-sized refractory oxides (ilmenite and Cr-spinel) and Fe-sulphide decorating their grain boundaries (Fig. 1D). Where anhydrous silicates are preserved, they are almost universally Mg-rich olivine (Mg# > 90 and generally Mg# > 96 – where Mg# is calculated as: Mg/(Mg + Fe) atomic ratios, Fig. 2 and Fig. S7). Silicate glass is absent, and pyroxene is extremely rare (Fig. 1F). Chondrule Fe-Ni-metal survives only as poikilitic grains held within olivine crystals.

The extent of aqueous alteration in B-7904 and Dho 1988 is less extreme than in Y-86720 and Y-86789. As a result, chondrules are more easily identified and their primary accretionary textures are better preserved. In B-7904, porphyritic chondrules are dominant although single crystal varieties are also common. Barred olivine and radiating pyroxene varieties are rare (Fig. 1). No cryptocrystalline chondrules were observed. Large angular isolated olivine grains, which are closely associated with chondrules (Jacquet et al., 2021), are abundant in B-7904. Owing to the less advanced state of aqueous alteration, B-7904 preserves some Fe-rich olivines (Mg# 55–88).

Chondrules (including heavily altered and pseudomorphic forms) represent between 7.1 area% (Y-86789) and 18.4 area% (B-7904) (Table 1). Sizes follow a skewed normal distribution with a long tail extending to large size fractions (Fig. 3, Fig. S8). Diameters range from ~50–1,525 μm with a mean of 340 μm, a median of 280 μm and a modal average of 200 μm.

Because CAIs are Poisson distributed, Hezel et al. (2008) concluded that the statistical analysis of CAI abundance in chondritic meteorites is unreliable when only small surface areas (<1,000 mm^2) are investigated. Our data supports this conclusion, most sections contain very few CAIs (<1 area%) with apparent diameters between 200 and 700 μm. However, the CY2 Dho 1988 is an exception where the presence of three CAIs with apparent diameters between ~500 and 1600 μm compose ~10 area% of the studied section. Rare pseudomorphic CAIs (outlines of former CAIs) are present with the CY1s. An example of aqueously altered former CAI within Y-82162 is shown in Fig. S9. Its presence is inferred based on the local enrichment in Ca and occurrence of a thin (<5 μm) fine-grained rim.

3.3. Fine-grained matrix

Like the CM and CI chondrites, the CY chondrites are dominated by

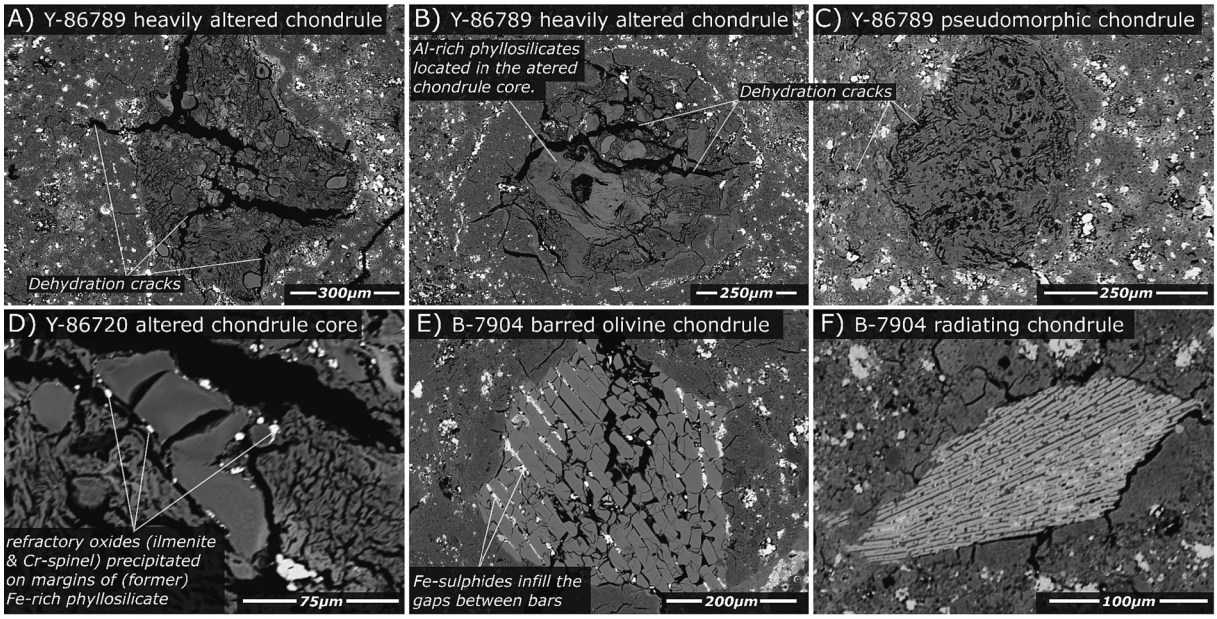

Fig. 1. Backscattered electron images of altered chondrules found in the CY2 chondrites. Panels A and B feature large heavily altered chondrules whose cores preserve relict textures, revealing the former existence of coarse fibrous phyllosilicates. The bright region in the core of B is composed of Al-rich phyllosilicates. Rounded nodular and Fe-rich phyllosilicates are visible in both chondrules. Panel C shows a pseudomorphic chondrule, also a common feature in the CY chondrites. Panel D shows a magnified region within an altered chondrule core, the bright phases adhering to the edge of the phyllosilicate grain are ilmenite and Cr-spinel grains. Panel E shows a mildly altered barred olivine chondrule, note the absence of interstitial chondrule glass. Instead Fe-sulphide minerals have formed between olivine lamellae. Panel F shows a rare radiating pyroxene chondrule fragment.

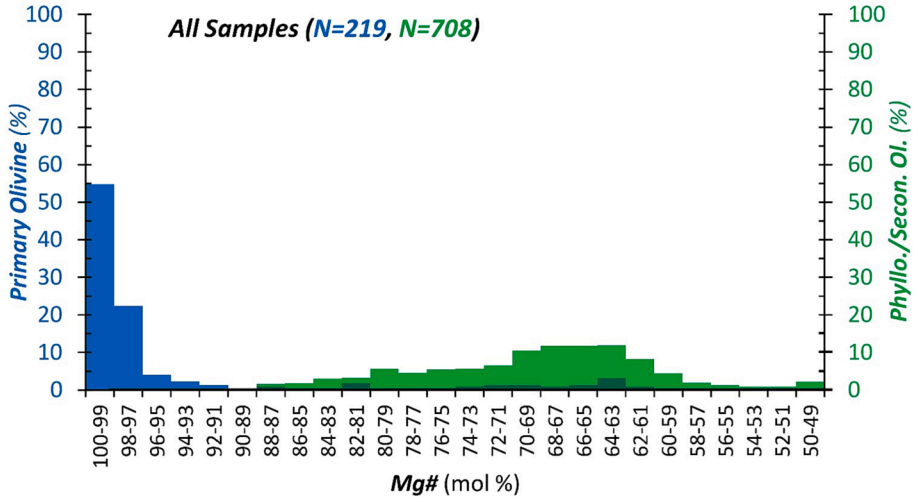

Fig. 2. Histogram illustrating the variation in olivine cation chemistry among the CY chondrites. Note data from all six meteorites are combined (individual plots for each meteorite are shown in Fig. S7). Primary olivine is plotted in (translucent) blue while secondary olivine (representing former phyllosilicates that subsequently recrystallized as olivine during thermal metamorphism) are plotted in (translucent) green. The two datasets overlap producing the mixed-shading seen.

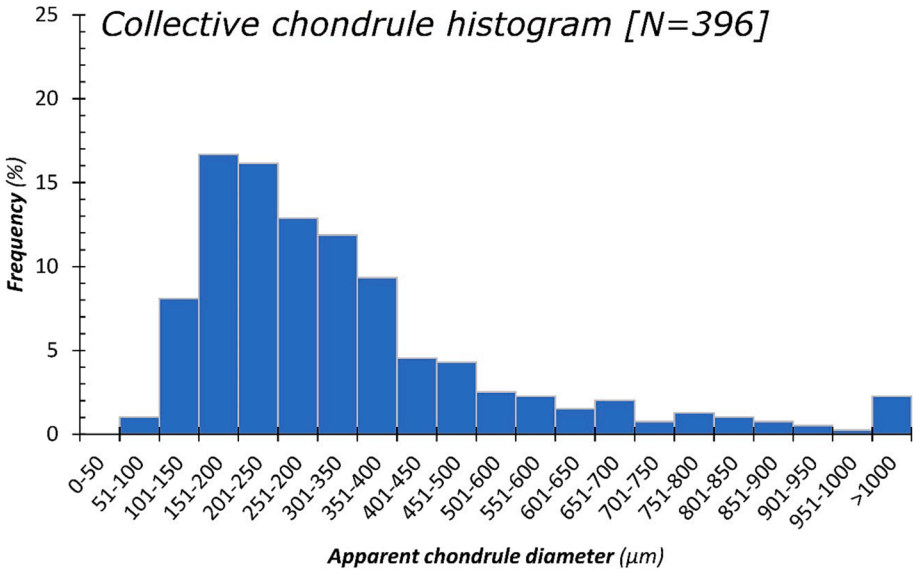

Fig. 3. Collective chondrule size distribution among the four CY2 chondrites. Diameters vary between 55 μm and 1525 μm. The mean average chondrule diameter is 340 μm, the median average is 280 μm and the modal average is 200 μm. Equivalent plots for each individual CY2 meteorite are shown in Fig. S8.

fine-grained matrix, with abundances varying between approximately 75–90 area%. Phyllosilicate minerals comprise the bulk of the matrix material, but owing to post hydration thermal metamorphism, these phases experienced dehydration, amorphization and, in most instances recrystallization, leaving a poorly crystalline groundmass of secondary olivine (Akai, 1990; 1992; Ikeda, 1992; King et al., 2019; Suttle et al., 2021a). Dehydration cracks (Fig. 1A–C), reflecting volume loss associated with dehydration of former phyllosilicates, are common features and clearly resolvable in localized regions of matrix. Elemental analysis of the matrix allows the approximate composition of former phyllosilicate minerals to be inferred. Combined Si + Al concentrations vary between 10 and 22 at.% and indicate the (former) presence of both serpentine and saponite (Fig. 4). High Na concentrations (0–4 at.%) are also common and correlate with increasing Si + Al, implying the existence of Na-saponite minerals (Fig. 4). Al-rich phyllosilicates (Al: 4–10 at.%) are found only in the CY2 chondrites. They have modest Fe contents (Mg# 68 ± 5.0 (1σ)) and low Na contents (avg: 1.1 at.%) and are interpreted as chlorite. This phase occurs only in the cores of some altered chondrules (Fig. 1B). In addition to those described above, the CY1s also have coarse phyllosilicate mineral clumps (Fig. 5A and B) reaching sizes of 100–300 μm. These clumps have high Na contents (Na > 1.5 at.%), and Mg-rich compositions (Mg#: 70 ± 10 (1σ)), and may contain embedded magnetite platelets and sulphides, as well as dense rims of magnetite (Fig. 5A).

3.4. Sulphides, metal and magnetite

All of the meteorites investigated in this study contain abundant Fe-sulphides (Fig. 6, overwhelmingly these are members of the pyrrhotite-troilite solid solution, and primarily have (Fe + Ni/S) atomic ratios close to the stochiometric ideal for troilite). Small-scale inclusions of pentlandite are present in some sulphide grains. They vary greatly in size and morphology from coarse aggregates (>250 μm in diameter) to small submicron grains embedded in the fine-grained matrix. Euhedral tabular sulphide laths are relatively common in the CYs and produce a distinctive texture in several of the meteorites. They are abundant in both CY1s

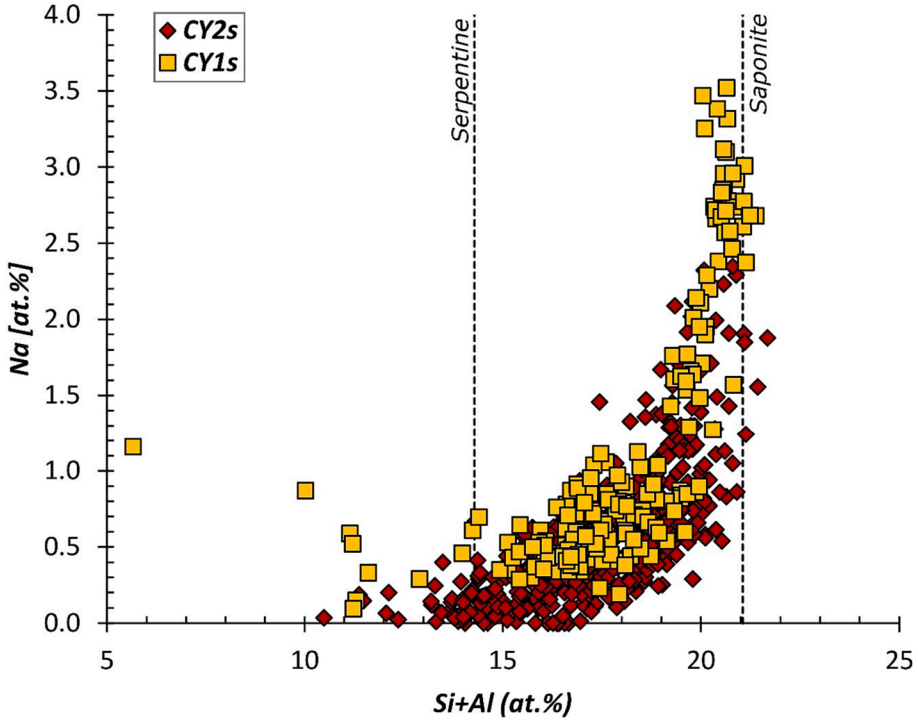

Fig. 4. Inferring (former) phyllosilicate cation composition and species from matrix EDX analyses. Data from all six CY meteorites are combined. CY2 data are shown as red diamonds and CY1 data as orange squares. The stochiometric ideal compositions for serpentine and saponite are marked by vertical dashed lines. Both petrologic subtypes of CY chondrite contain a mix of serpentine and saponite although saponite is more common in the CY1s. Saponite minerals have elevated Na abundances, indicating the former presence of Na-saponite.

and in two of the CY2s (Y-86720 and Y-86789), however, laths are less common in the two least aqueously altered meteorites (the CY2s: B-7904 and Dho 1988). Instead, the large sulphides in these meteorites have rounded morphologies and irregular shapes. Elemental analysis (WDS) of the larger (>5 μm) Fe-sulphides in the CY2s reveal consistent compositions with low Co (<0.7 wt%), low Cr (<0.8 wt%) and low Mn (<0.1 wt%) concentrations but variable Ni (generally < 12 wt% (equivalent to ~14 at.%), Fig. 6, Fig. S10). Ni and Co abundances are weakly correlated with Ni/Co (wt.%/wt.%) ratios varying between 0 and ~300 and a median average value of 4. For the CY1s, Fe-sulphide compositions are similar with low Co (<0.5 wt%), low Cr (<0.8 wt%) and low Mn (<0.1 wt%) and Ni < 7.3 wt% (Fig. 6). Ni and Co abundances are more strongly correlated than in the CY2s – Ni/Co (wt.%/wt.%) ratios in the CY1s vary between 2 and 37, with a median average value of 14.

Metal occurs as an accessory phase in the CYs and primarily as small grains embedded within Fe-sulphides (either completely enclosed or partially exposed at the grain margin (Fig. 7)). Metal is also rarely present within chondrule olivines. Fe-sulphide-hosted metal grains are small (<15 μm) with anhedral morphologies and variable compositions. Both kamacite (Ni < 10 at.%) and taenite (Ni > 10 at.%) are found in the CY2s, whereas only taenite is preserved in the CY1s (Fig. 6). Taenite contains Co with abundances <3 wt% (Table 2).

Magnetite is identifiable only in the CY1s and occurs with a range of morphologies including as small crystals dispersed within the matrix, as platelets and as grain clusters (Fig. 5). Magnetite grains typically contain both Mn (<2.5 wt%) and Mg (<3.0 wt%) (Table 2). Both CY1s have several large (~200 μm) dense magnetite clusters composed of coarse, subhedral magnetite crystals embedded within a fine-grained phyllosilicate (Mg# ~65) and co-occurring with occasional small (~10 μm) Ca-phosphate grains (Fig. 5). Most of these magnetite clusters have a clearly defined rim of Mn-bearing (Mn: 0.8–1.6 wt%) phyllosilicate material.

3.5. Phosphates

Phosphates, in the form of apatite, are present in all the CYs, where they occur as an accessory phase (Table 2) and typically, in close association with Fe-sulphides. In the CY2s they have anhedral morphologies and survive as a series of residual grains typically <10 μm in size. In B-7904 they occur as a thin discontinuous rim on a radiating pyroxene chondrule. Conversely, in Y-86789 they have Mg-rich compositions whose textures reveal the former outlines of much larger phosphate minerals and appear to occupy fractures, forming infilled mineral veins (Fig. S11). Phosphates are more abundant in the CY1s, appearing as larger grains, again identified as apatite but preserving euhedral morphologies. Apatite in the CY1s is typically found in association with phyllosilicate and magnetite (Fig. 5) or alone embedded within the fine-grained matrix.

3.6. Carbonates

Carbonates are present in the CY1s where they co-occur with magnetite. In Y-86029 (CY1) a single loose cluster of carbonate minerals was observed (Fig. 8B and 8C) with a mottled texture. By contrast, thermally decomposed Ca-rich masses, interpreted as former carbonate minerals, are found in the CY2s in association with sulphides (Fig. 8E and in Suttle et al., 2021a). They commonly occur as infill material forming veins and vugs (Fig. 8D and F). Thus, there are (at least) two distinct generations of carbonate formation in the CYs. For both the CY1s and CY2s elemental analyses reveal low Fe concentrations (<5 at.%), but variable Ca and Mg contents (Fig. S12) with compositions corresponding to both calcite and dolomite. (Combined four-element EDX maps showing Ni, S, Ca and P distribution help reveal the occurrence of apatite, carbonates and Fe-Ni-sulphides. These are given in the supplementary material with sections Y-86029, Y-86720 and Y-86789 (Figs. S13, S14 and S15 respectively) shown as examples).

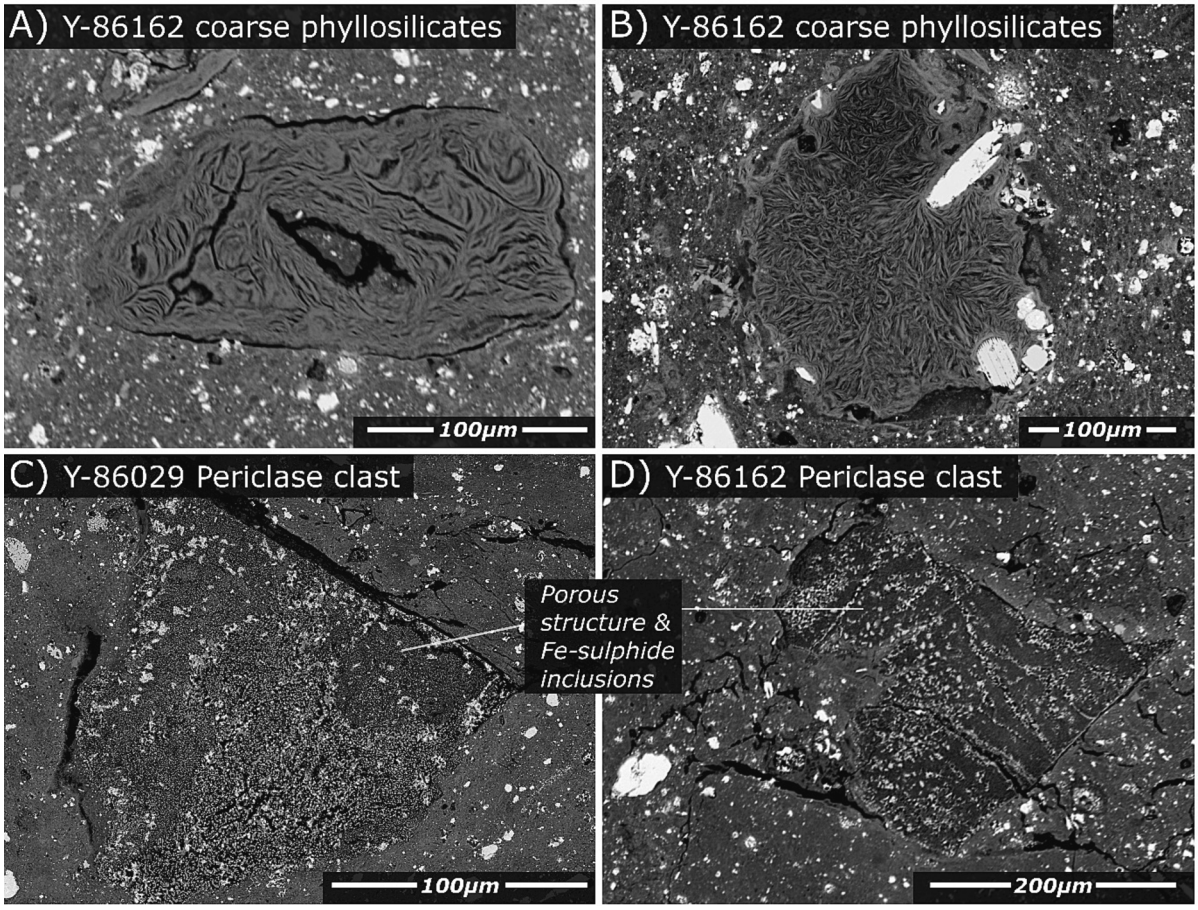

Fig. 5. Backscattered electron images of unique phases found in the CY1 chondrites. Panels A and B show coarse phyllosilicate clumps, while panels C and D show examples of ferropericlase clasts.

3.7. Refractory oxides

Refractory oxides (Cr-spinel and ilmenite) are present in the CY2s. Two distinct generations are recognizable based on texture and grain size. The first generation are euhedral grains (<30 μm) primarily found in chondrule cores. The second generation occurs as micron and submicron-sized crystallites with anhedral morphologies, located only on the edges of coarse phyllosilicate (and former phyllosilicate) minerals. Spot EDX analyses reveal different compositions (Fig. 9).

3.8. Ferropericlase

Ferropericlase is an Fe-Mg oxide ([Fe,Mg]O) not reported in other carbonaceous chondrites, but previously identified in the CY1s (Ikeda, 1992; King et al., 2019). We found ferropericlase clasts only in the CY1s, Y-86029 and Y-82162 (Fig. 5C and D). They appear as large (>150 μm) irregular-shaped objects with high porosity (visible in BSE images and evidenced by low EDS totals). Grain interiors contain Fe-oxide inclusions and are cut by abundant subparallel fracture sets and infilled with small Fe-sulphide grains (Fig. 6C and D).

3.9. Raman on carbonaceous phases

Carbonaceous materials feature Raman bands in the first- and second-order regions. The most typical peaks are the first-order defect (D) band at ~1350–1380 cm^{-1} and the graphite (G) band at ~1580–1590 cm^{-1} (Tuinstra and Koenig, 1970). The peak parameters of the D and G bands including the peak position (ω), peak widths in terms of full width half-maximum (FWHM, Γ), and the peak intensity ratios between the D and G bands (I_D/I_G) of the CY group meteorites, compared to other carbonaceous and ordinary chondrites are shown in Table S1, and the data is plotted in Fig. 10. In this figure data for the CY chondrites are plotted as black symbols for their easy identification from the other chondrites shown. (Dho 1988 is not included in the Raman dataset because we have not observed any carbonaceous features in this sample).

The peak parameters of the D and G bands are systematically correlated with the maturation of organic matter (Fig. 10, Table S1). The combination of peak parameters describes the overall size distribution of the crystalline domains and the metamorphic history of the carbonaceous host (e.g., Busemann et al., 2007; Bonal et al., 2006; Chan et al., 2019a, 2019b). For example, ω_D and Γ_D values are low in heated meteorites, as seen for Allende, which has experienced peak metamorphic temperature (PMT) of >600 °C and has low ω_D and Γ_D values of 1,351.5 ± 1.2 cm^{-1} and 62.5 ± 1.9 cm^{-1}, respectively (Table S1). This contrasts with the high values (ω_D = 1,378.5 ± 11.1 cm^{-1}; Γ_D = 370.8 ± 54.2 cm^{-1}) observed for primitive (CM, CI) meteorites like Mighei and Ivuna, which were estimated to have been heated <220 °C. The strong correlation between the Γ_D and PMT has been observed and developed into a cosmothermometer for the estimation of PMTs of astromaterials (Busemann et al., 2007). Fig. 10A plots ω_D vs. Γ_D values; here, the CY chondrites (both CY2s and CY1s) plot halfway between the nominally unheated CI Ivuna and the heated CV3 Allende. The position of the CY group implies an intermediate maturity stage and, therefore, some heating. Within the CYs, the maturation grade of the organic matter suggests the following metamorphic hierarchy from least to most thermally processed: Y-82162 (CY1) < Y-86029 (CY1) ≤ B-7904 (CY2) ≤ Y-86789 (CY2) ≤ Y-86720 (CY2). Notably, the CY2s have higher

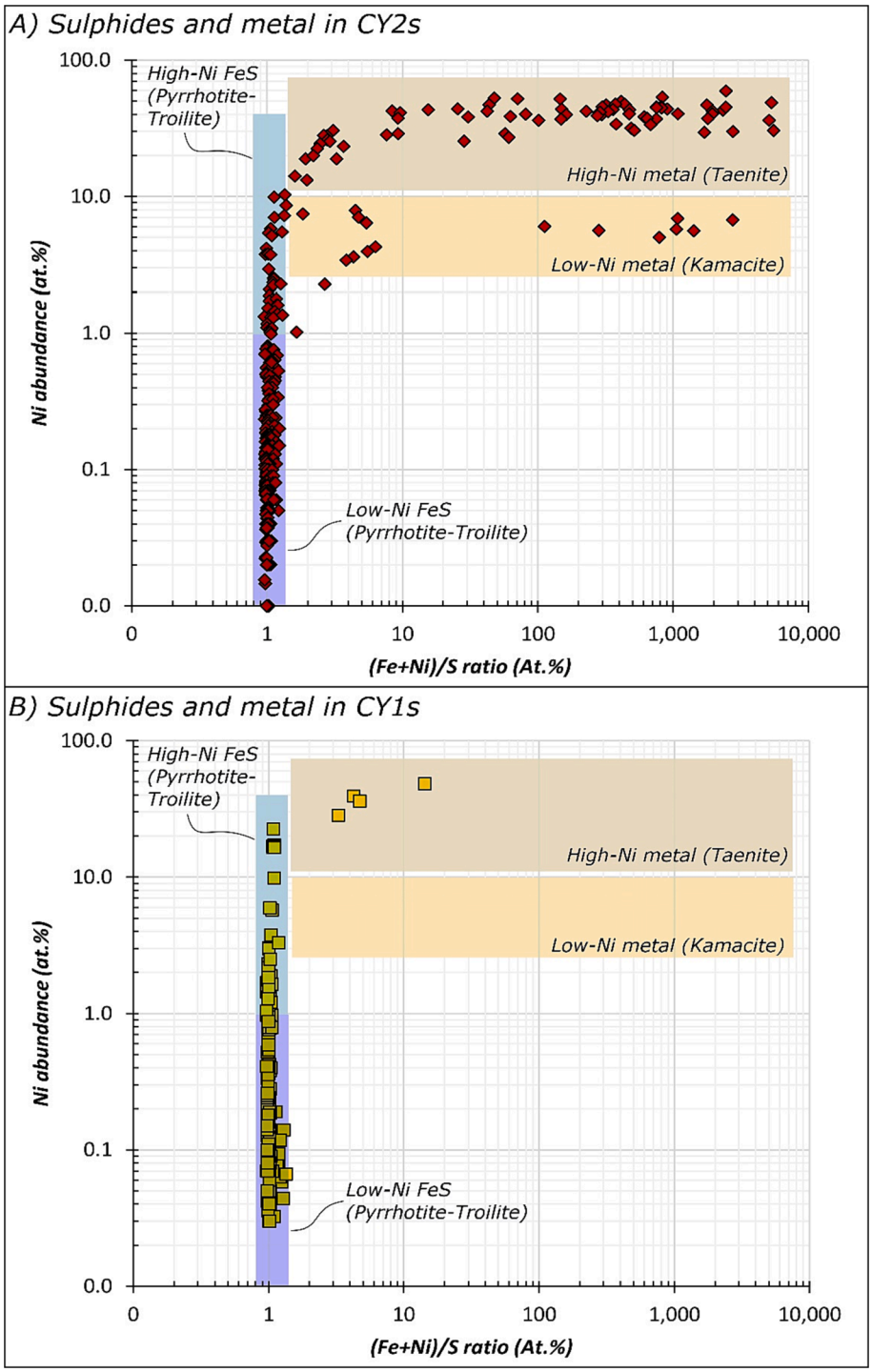

Fig. 6. Chemical compositions of Fe-sulphide and Fe-Ni-metal in the CY chondrites. This graph plots the cation/S ratio against Ni abundance, with data presented in atomic %. (Fe+Ni)/S ratios close to 1 represent sulphide minerals, while ratios >1 indicate metal phases (containing minor dissolved S). The compositional ranges of low-Ni metal (kamacite < 10 at.%) and high-Ni metal (taenite > 10 at.%) are shaded and labelled. Panel A depicts data from the four CY2 chondrites (shown as red diamonds), while panel B depicts data from the two CY1s (shown as orange squares). Surviving metal is rare in the CY1s and occurs only as taenite.

maturation grades and, therefore, either longer duration heating or higher peak temperatures relative to the more aqueously altered CY1s.

The Raman graphite band width of chondritic organic matter, modified by short-term heating has been observed to differ significantly from that modified by long-term metamorphic heating (Chan et al., 2019a). The Γ_G values of the organic material in CY group meteorites, ranging from 87.8 ± 6.3 cm^{-1} in Y-86720 up to 123.0 ± 11.3 cm^{-1} in Y-82162, are distinctively larger than those in other carbonaceous and ordinary chondrites (<76 cm^{-1}) (Fig. 10C and D). Accordingly, the ω_G values of the CY chondrites, ranging from 1,616.5 to 1,623.2 cm^{-1}, are also higher than those observed for most of the other chondrites (<1607.9 ± 1.4 cm^{-1}), except only for Huacachina (LL3), of which the ω_G value (1,617.2 ± 1.9 cm^{-1}) is more comparable to Y-86029 (CY1) and Y-82162 (CY1) (1,617.0 ± 2.0 cm^{-1} and 1,616.5 ± 2.9 cm^{-1}, respectively) (Fig. 10D). The trend observed in the Γ_G values correlates to the Γ_D values, where samples showing high Γ_D values exhibiting low

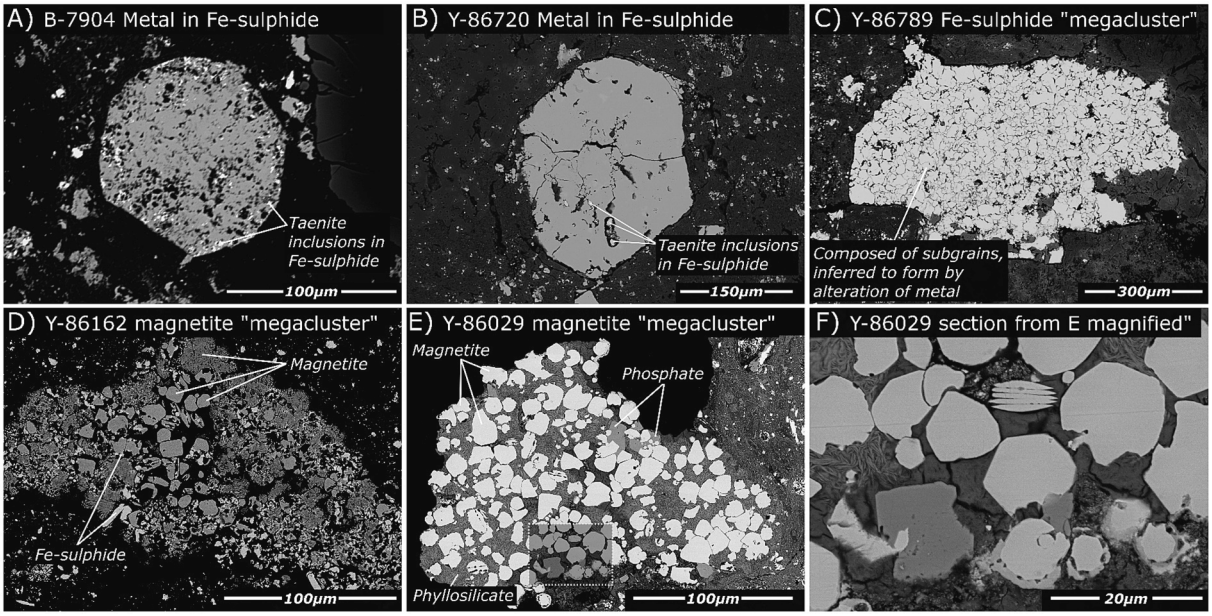

Fig. 7. Backscattered electron images of sulphides, magnetite and metal in the CY chondrites. A-C show images of Fe-sulphides in the CY2s, metal can be identified as residual bright spots, appearing as inclusions within Fe-sulphides (A and B). Rare large aggregates of Fe-sulphide (megaclusters) are present in the CY2s. D-F show images of magnetite aggregates found only in the CY1s. They are composed of magnetite plus phyllosilicates, apatite and residual Fe-sulphide and are interpreted as having formed by aqueous alteration of the Fe-sulphide aggregates seen in the CY2s.

Γ_G values, following the order Y-82162 (CY1) > Y-86029 (CY1) > B-7904 (CY2) > Y-86789 (CY2) > Y-86720 (CY2).

4. Discussion

4.1. Chondrules in the CY group

Analysis of the less-altered CY2s provides insights into the primary accretionary properties of the CY chondrites. B-7904 and Dho 1988 are the least aqueously altered CY2s, and their chondrule outlines are clearly defined and easily resolvable. These meteorites also have the highest chondrule abundances of 18.4 area% (B-7904) and 15.2 area% (Dho 1988). In the more altered CY2s, estimated chondrule abundances are lower (7.1 area% and 9.6 area%). Conversely, in the CY1s chondrules are absent, and chondrule pseudomorphs were not definitively identified. These relationships developed as progressive aqueous alteration replaced the primary mineralogy, metasomatizing chondrule outlines. Chondrule abundances in B-7904 and Dho 1988 (Fig. S8) are, therefore, most representative of the initial parent body and suggest that a theoretical initial CY3 parent body accreted chondrules at abundances between 15 and 20 area%. Chondrule size estimates are fairly consistent between each of the samples analysed, except for Dho 1988, which contains some larger chondrules, skewing the mean calculation. However, we note that the relatively low number of chondrules (N = 38) in our Dho 1988 section means that its values are affected by small sample statistics. The combined mean average apparent chondrule diameter in the CY2s is 340 μm, or 320 μm if the data from Dho 1988 are excluded.

This size is slightly larger than the average for CM chondrites, typically quoted as between 270 and 300 μm (Rubin and Wasson, 1986; Weisberg et al., 2006). The larger chondrules in Dho 1988 could be a product of sampling a relatively small section area (65 mm^2) or could indicate that Dho 1988 is somewhat distinct from the other CY2s. Dho 1988 also includes relatively large CAIs, which are otherwise unsampled in the other sections, suggesting that the latter may apply. This observation may also suggest that size sorting processes affected the region of space where the CY chondrites accreted (Wurm and Krauss, 2006) or size sorting after accretion whilst on the parent body (e.g. Pinto et al., 2021).

4.2. Brecciation predates aqueous alteration

Several of the CYs have a brecciated texture. This is most pronounced in Y-86029 (CY1) and Dho 1988 (CY2). Previously, Suttle et al. (2021a) concluded that brecciation in Dho 1988 predated the main episode of aqueous alteration. This interpretation was based on the presence of veins composed of phyllosilicate, carbonate and sulphide minerals infilling fractures separating clasts, indicating that significant aqueous alteration occurred after fragmentation. Analysis of Y-86029 suggests a similar chronology. Although this meteorite lacks mineralized veins, the boundaries between clasts are diffuse, implying that post-brecciation alteration formed hydrous minerals that blurred the otherwise sharp contacts between fragments through geochemical exchange and mineral formation. In Y-82162, several small clasts are discernible, held within a main lithology (Fig. S2). Boundaries between clast and host lithology are often separated by thin open fractures. However, in many instances these boundaries completely lack fractures and are instead transitional. The absence of brecciation in the remaining three CY2s (B-7904, Y-86720 and Y-86789) studied implies either these samples escaped brecciation or that clast sizes are larger than the sampling scale of the section we have evaluated. In either instance, the lack of brecciation means we are unable to evaluate the relative chronology of brecciation and alteration in these meteorites. Nonetheless, the three brecciated CYs reveal the same geological history, either brecciation followed by aqueous alteration or aqueous alteration punctuated by brecciation. In both scenarios, aqueous alteration was active after fragmentation. This contrasts with the apparent alteration histories of the CM chondrites, in which there are typically sharp contacts between lithological clasts and often a disparate range of alteration extents found in close proximity (Nakamura et al., 1999; Verdier-Paoletti et al., 2017; Lentfort et al., 2021; Suttle et al., 2023). The textures in CM chondrites, therefore, require that brecciation postdates fluid activity, potentially by millions of years (e.g. Amsellem et al., 2020).

4.3. Reconstructing the aqueous alteration history of the CY group

Analysis of the CY2s provides evidence for the early stages of hydration, while the CY1s record more advanced, late-stage aqueous

Table 2
Elemental compositions (expressed as uncorrected weight totals [wt.%]) for various phases analysed in this work. The "†" symbol denotes EDS analyses, the remainder are WDS analyses

Phase	Setting	Analysis	N=?	Na	Mg	Al	Si	P	S	Cl	K	Ca	Ti	V	Cr	Mn	Fe	Ni	Co	O	Total
Chlorite (at.%: Al > 4)	CY2s	*Avg.*	67	1.2	14.1	7.8	16.5	–	–	–	0.2	0.2	0.1	–	0.5	0.1	14.9	0.1	–	40.8	97.0
		Stdev.		*0.6*	*1.8*	*2.0*	*1.5*	–	–	–	*0.1*	*0.5*	*0.1*	–	*0.4*	*0.1*	*2.5*	*0.2*	–	*1.8*	*4.2*
Na-Saponite (at.%: Na > 1)	CYs	*Avg.*	99	1.9	15.4	2.6	19.6	–	–	–	0.2	1.2	–	–	0.6	0.2	9.0	0.1	–	39.7	91.0
		Stdev.		*0.8*	*1.9*	*1.0*	*5.3*	–	–	–	*0.1*	*3.9*	–	–	*0.6*	*0.3*	*3.5*	*0.2*	–	*4.0*	*6.0*
Serpentine (at.%: Si + Al < 17)	CYs	*Avg.*	244	0.3	14.9	1.4	15.7	–	–	–	0.1	1.0	0.1	–	0.5	0.3	17.5	1.2	0.1	35.6	88.7
		Stdev.		*0.2*	*3.5*	*0.6*	*2.5*	–	–	–	*0.1*	*2.0*	*0.1*	–	*0.5*	*0.4*	*5.9*	*1.0*	*0.1*	*4.0*	*7.9*
Taenite†	CY2 (B-7904)	Single	1	–	–	–	–	–	–	–	–	–	–	–	0.1	–	37.4	60.7	1.5	–	100.0
Kamacite†	CY2 (Y-86720)	Single	1	–	–	–	0.1	–	–	–	–	–	–	–	0.1	–	93.7	5.9	0.4	–	100.3
Fe-sulphide	CY2s	*Avg.*	150	–	0.2	–	0.2	–	35.7	–	–	0.1	–	–	–	–	62.8	0.6	–	–	99.7
		Stdev.		–	*0.2*	*0.1*	*0.2*	–	*1.4*	–	–	*0.1*	–	–	*0.1*	–	*2.1*	*1.7*	*0.1*	–	*1.9*
Fe-sulphide	CY1s	*Avg.*	92	–	0.4	–	0.3	–	35.9	–	–	–	–	–	0.1	–	61.8	0.9	0.1	–	99.6
		Stdev.		–	*0.8*	*0.1*	*0.5*	–	*1.5*	–	–	–	–	–	*0.1*	–	*2.5*	*1.2*	*0.1*	–	*2.1*
Mg-apatite†	CY2 (Y-86789)	*Avg.*	13	3.1	19.8	0.5	0.3	20.8	–	–	–	2.9	–	–	–	0.2	6.1	0.1	–	44.8	98.5
		Stdev.		2.1	3.0	0.6	0.4	1.2	–	–	–	2.1	–	–	–	0.1	1.9	0.1	–	*2.1*	*4.4*
Apatite†	CY2 (B-7904)	*Avg.*	6	1.7	2.8	0.4	1.9	16.3	0.5	–	0.1	27.6	–	–	0.1	0.1	5.6	0.7	–	42.1	99.9
		Stdev.		*0.3*	*1.2*	*0.3*	*1.5*	*3.0*	*0.6*	–	–	*5.2*	–	–	*0.1*	–	*3.6*	*0.9*	–	*2.3*	*2.9*
Apatite†	CY1s	*Avg.*	37	0.2	0.4	0.1	0.5	16.8	0.2	0.1	–	36.5	–	–	–	0.1	1.9	0.1	–	39.4	96.4
		Stdev.		*0.1*	*0.6*	*0.1*	*0.5*	*1.2*	*0.4*	*0.2*	–	*2.5*	–	–	–	*0.1*	*2.6*	*0.1*	–	*2.6*	*3.0*
Primary Cr-spinel†	CY2s	*Avg.*	25	–	3.3	4.2	0.5	–	–	–	–	0.1	0.7	0.4	36.5	0.3	22.2	0.1	–	30.3	98.6
		Stdev.		*0.1*	*1.5*	*3.1*	*1.0*	–	–	–	–	*0.1*	*0.3*	*0.2*	*5.0*	*0.1*	*3.1*	*0.1*	–	*1.8*	*1.7*
Secondary Cr-spinel†	CY2s	*Avg.*	25	0.3	6.5	1.0	5.4	0.1	0.4	–	–	0.2	0.1	0.1	31.1	0.3	18.3	0.2	–	31.8	95.8
		Stdev.		*0.3*	*2.5*	*0.6*	*2.4*	*0.1*	*0.8*	–	–	*0.3*	*0.1*	*0.2*	*6.7*	*0.1*	*2.9*	*0.2*	–	*2.9*	*5.1*
Primary Ilmenite†	CY2s	*Avg.*	37	0.1	2.7	0.1	0.5	0.1	0.1	–	–	0.2	30.6	0.2	0.1	0.7	30.7	0.1	–	32.4	98.4
		Stdev.		–	*0.6*	*0.1*	*0.6*	*0.1*	*0.1*	–	–	*0.2*	*1.5*	*0.1*	*0.1*	*0.3*	*1.0*	*0.1*	–	*0.6*	*1.7*
Secondary Ilmenite†	CY2s	*Avg.*	8	0.2	7.7	0.5	3.8	0.1	–	–	–	0.1	25.1	0.1	0.4	0.3	24.3	0.1	–	35.0	97.7
		Stdev.		*0.1*	*1.0*	*0.3*	*1.2*	–	–	–	–	–	*3.0*	*0.1*	*0.1*	*0.1*	*1.2*	–	–	*2.1*	*3.8*
Magnetite†	CY1s	*Avg.*	68	0.1	0.9	0.1	0.1	–	0.1	–	–	0.2	–	–	–	1.0	67.3	0.1	–	20.6	90.4
		Stdev.		*0.1*	*0.6*	*0.1*	*0.1*	–	*0.1*	–	–	*0.2*	–	–	–	*0.8*	*1.5*	*0.1*	–	*0.4*	*0.9*
Ferropericlase†	CY1 (Y-86029)	*Avg.*	14	–	23.8	0.3	0.3	–	0.4	0.1	–	0.2	–	–	–	1.2	20.1	0.1	–	23.1	69.7
		Stdev.		–	*2.0*	*0.2*	*0.2*	–	*0.3*	–	–	–	–	–	–	*0.3*	*2.0*	*0.1*	–	*1.5*	*3.3*
Ferropericlase†	CY1 (Y-82162)	*Avg.*	18	0.1	27.0	0.8	0.3	–	2.0	0.1	–	0.2	–	–	–	2.6	14.5	0.1	–	27.0	74.8
		Stdev.		–	*0.9*	*0.5*	*0.1*	–	*1.6*	–	–	*0.1*	–	–	–	*0.8*	*2.5*	*0.1*	–	*3.6*	*8.7*

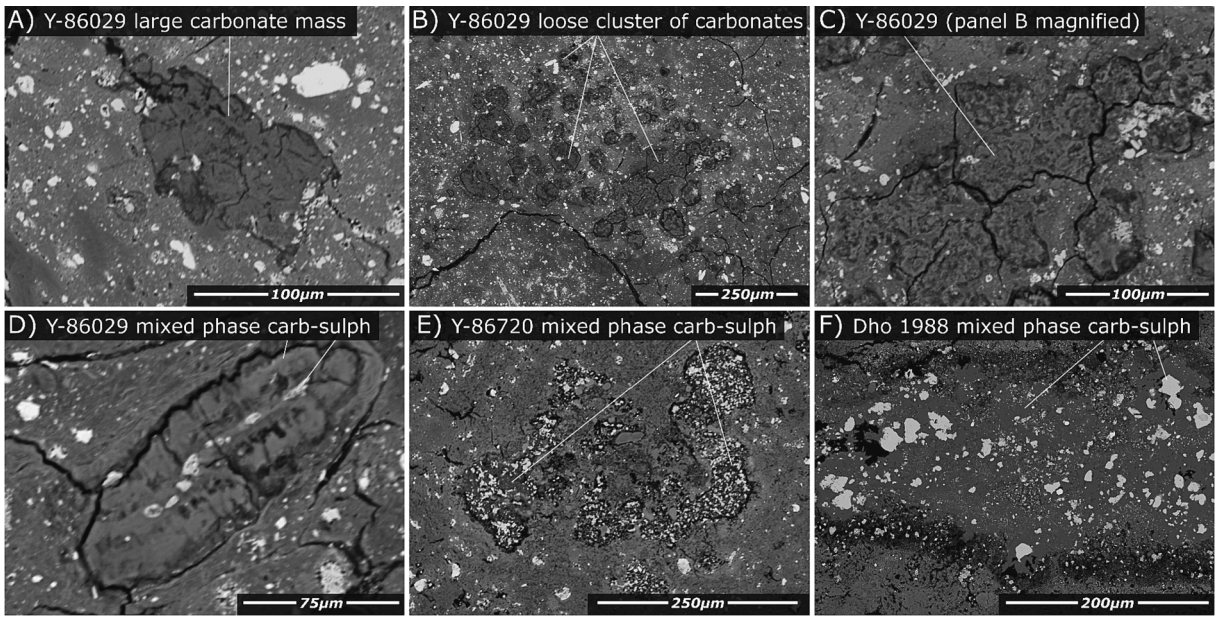

Fig. 8. Backscattered electron images of carbonates/former carbonate phases in the CY chondrites. Panels A-D show carbonates in CY1s while panels E and D show carbonates in CY2s. Panel A typifies a single carbonate mass. Panel B shows a loose cluster of carbonate grains (magnified in C). Panel D shows a small vein infill, representing a mixed phase assemblage of carbonate and sulphide that has infilled void space during aqueous alteration. Panel E shows an irregular-shaped mass composed of carbonate and sulphide. Panel F shows a large and layered mineralized vein, the outer edge is composed of phyllosilicate while the inner region is mixed phase carbonate-sulphide. Note most carbonate have suffered partial or complete decomposition during post hydration thermal metamorphism.

alteration. The presence of a pseudomorphic CAI in the CY1 Y-82162 (Fig. S9) implies that the CY1s accreted refractory inclusions (chondrules and CAIs). However, their rarity in the CY1 lithology attests to intense alteration. Aqueous alteration in the CY chondrites followed a similar trajectory to the CM and CI chondrites, with Fe-Mg-bearing phyllosilicates and Fe-sulphides being the main minerals formed. Minor quantities of carbonates and magnetite are additional similarities. However, distinct differences occur in their phyllosilicate species, cation contents and accessory phases. Elemental analysis of the fine-grained matrix (Fig. 4, Table 2) suggests both serpentine and saponite were produced during alteration. This is distinct from the CM chondrites where typically only serpentine is found (Bunch and Chang, 1980; Howard et al., 2009), and is instead similar to the CI chondrites (Tomeoka and Buseck, 1988; Russell et al., 2022) and the C2-ungrouped Bells meteorite (Brearley, 1995). Additionally, elevated Na contents suggest that the saponite minerals included Na-saponite. Experimental studies have shown that, relative to serpentine, saponite forms at higher water-to-rock (W/R) ratios (Kikuchi et al., 2021) and/or under elevated silica activities (Brearley, 1995), under more alkaline conditions and at higher temperatures (Ohnishi and Tomeoka, 2007). The formation of Na-saponite may suggest that alkaline brines (Na-bearing fluids) were present during alteration (Zolotov, 2012). We also identified chlorite in the CY2s, located within altered chondrule cores. They would have formed from Al-bearing precursors such as feldspar and chondrule glass and are, therefore, evidence of former Al-bearing chondrules. However, their absence in the CY1s requires that early-formed chlorite was subsequently dissolved and replaced by saponite as alteration advanced (Zolotov, 2012).

Minimally altered CM chondrites are perhaps the closest analogue to the petrography of the type 3 CY accretionary assemblage. In the Asuka CM chondrites, nominally CM2.8–3.0 (Kimura et al., 2020) Fe-sulphides are present as submicron grains within the fine-grained matrix and as larger pyrrhotite-pentlandite intergrowths within chondrules. This differs from the coarse Fe-sulphide laths and rounded grains present in the CY chondrites. Their morphologies suggest that the majority of the Fe-sulphides are not pre-accretionary phases but were formed during parent body alteration. The aqueous alteration of chondritic Fe-Ni-metal can form either phyllosilicates (cronstedtite), sulphides (tochilinite and pyrrhotite) or oxides (magnetite and goethite) depending on the geochemical microenvironment of the altering fluids (Fig. 11A) (Palmer and Lauretta, 2011; Nadoll et al., 2014; Pignatelli et al., 2016; Suttle et al., 2022a). In the CM chondrites, evidence for all three alteration pathways can be found in the same meteorites, often in close proximity (<100 μm). During the alteration of metal up to 81% of the Fe is dissolved and carried elsewhere by the fluid phase (Palmer and Lauretta, 2011). We suggest that in the CY chondrites a significant fraction of the primary (accreted) Fe-Ni-metal was converted into Fe-sulphides. Rounded Fe-sulphide grains (e.g. Fig. 8A) are evidence for direct, pseudomorphic replacement of former metal beads. In addition, many of the large Fe-sulphide grains in the CYs are lath-shaped with hexagonal basal sections, which is the characteristic morphology of euhedral pyrrhotite formed by precipitation from Fe-rich/S-rich fluids and the dominant form of sulphide in the aqueously altered CI chondrites (Bullock et al., 2005), Ryugu sample return materials (Yamaguchi et al., 2023), ungrouped C1 Flensburg meteorite (Bischoff et al., 2021) and heavily altered CM chondrites (Kimura et al., 2011). These lath-shaped sulphides are, therefore, robust evidence of sulphide generation during aqueous alteration (Bullock et al., 2005; Schrader et al., 2021). Thus, an initial generation of Fe-sulphides would have formed during aqueous alteration, both by direct sulphidation of metal and by the dissolution of metal and later precipitation as new Fe-sulphide minerals into void space. If metal was the principal precursor for Fe-sulphides then the high abundances of Fe-sulphides (10–30 vol%, King et al., 2019) indicate that the unaltered primary CY3 assemblage contained significant quantities of metal, and in this respect would have been similar to the metal-rich CR3 chondrites (e.g. Abreu et al., 2020).

As aqueous alteration advanced, some of the Fe-sulphide population was converted into magnetite. Evidence for this is given by (1) the elevated magnetite abundances found in the CY1s relative to the CY2s (>2 vol% vs. <2 vol%, King et al., 2019) and (2) the presence of magnetite aggregates (Fig. 7E) or mixed phase magnetite-sulphide aggregates (Fig. 7D) found in the CY1s, while only sulphide aggregates are found in the CY2s (Fig. 7C). These features indicate a transition to more oxidizing conditions during the more advanced stages of aqueous

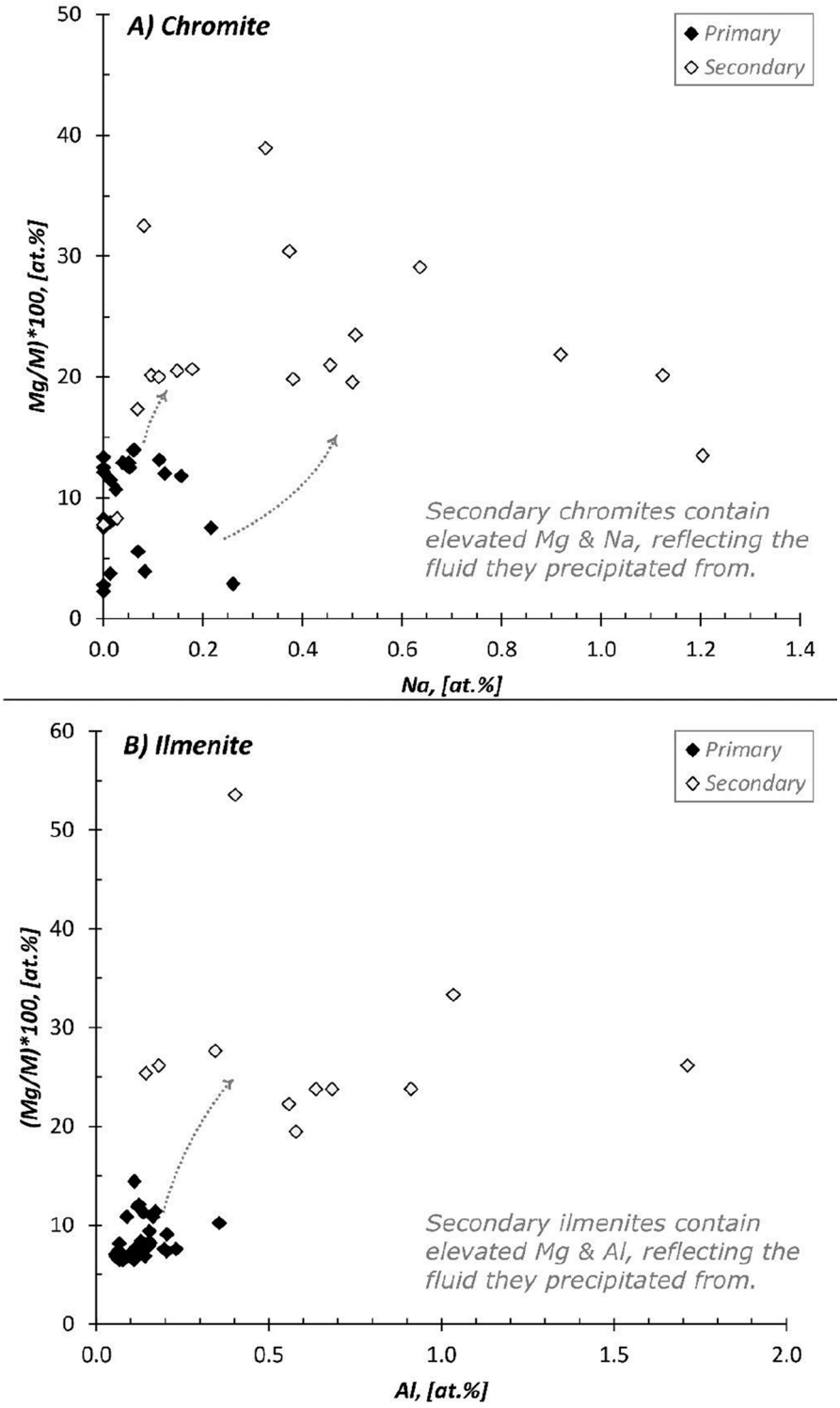

Fig. 9. The chemical compositions of refractory oxide minerals in the CY2s. Both (A) Cr-spinel and (B) ilmenite are found. In each case, there are two distinct generations: primary accretionary minerals (shown in black) and a second generation (shown in light grey), formed during aqueous alteration by precipitation from fluids. The primary oxides have low Mg concentrations and relatively pure compositions, while the secondary oxides incorporate Mg and trace elements, inherited from their parent fluids.

alteration (Fig. 11A), a feature inferred for the CM chondrites (Guo and Eiler, 2007; Le Guillou et al., 2015; Pignatelli et al., 2017; Vacher et al., 2019; Suttle et al., 2021b), CI chondrites (Alfing et al., 2019) and CR chondrites (Harju et al., 2014; Le Guillou et al., 2015).

Carbonates are present in at least two distinct settings. (1) Sulphide-carbonate clusters (Fig. 8A, D and F) and (2) magnetite-carbonate clusters (Fig. 8B and C). These different assemblages are interpreted as multiple generations of carbonate growth during aqueous alteration. Among the CY2s, only the sulphide-carbonate assemblages are present, while both the sulphide-carbonate and the magnetite-carbonate assemblages are present in the CY1s. Therefore, the sulphide-carbonate clusters appear to have formed earlier in the alteration sequence and

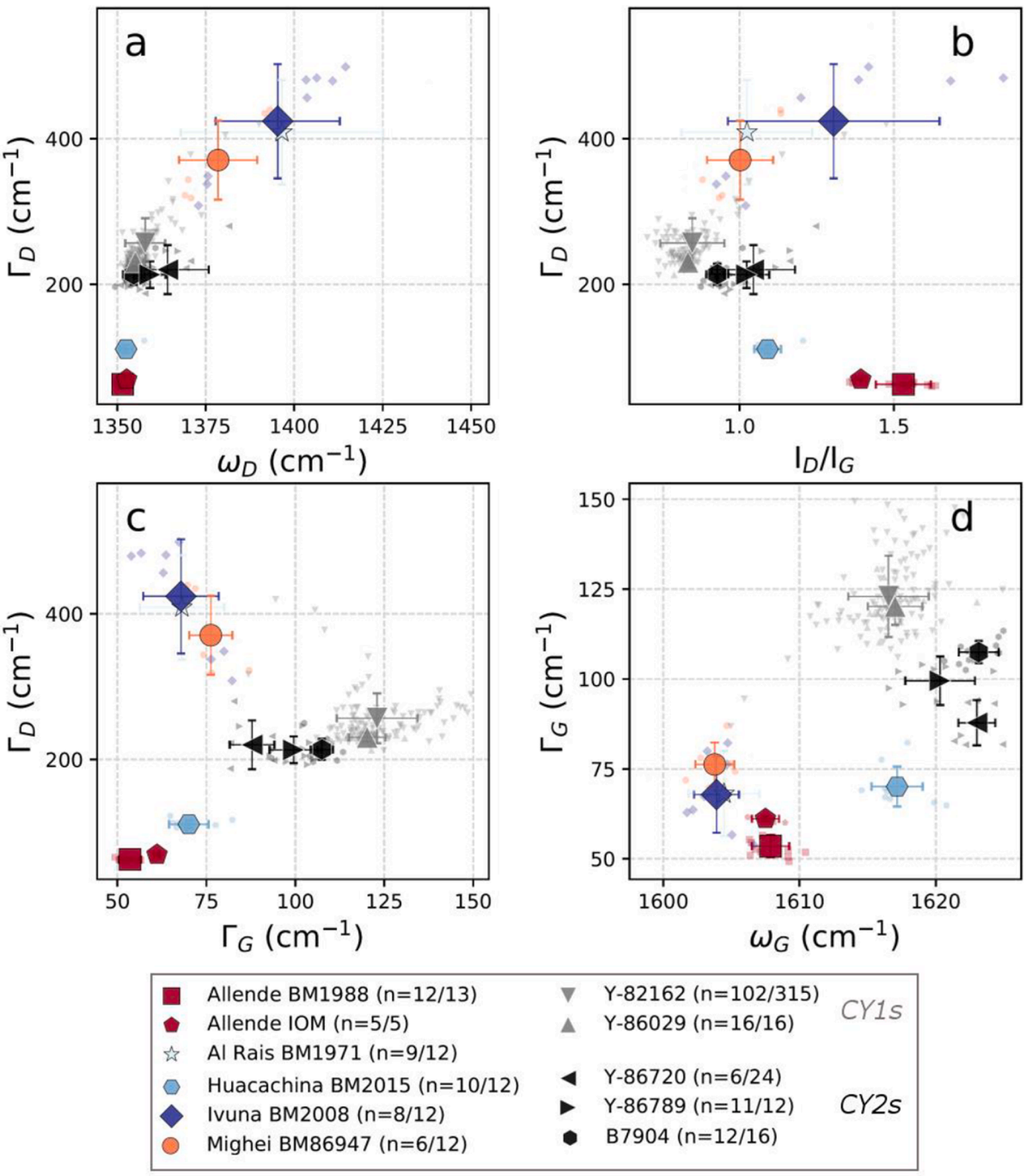

Fig. 10. Raman D- and G- band peak parameter data for the CYs chondrites studied in this work, and comparison with reference chondrites (CY1s are shown in grey and CY2s shown in black). Panels show, A: D-band parameters, B: the "R1" ratio of peak intensities, C: the relationship between D- and G-band FWHM and D: G-band parameters. The small grey symbols represent individual data points, while the larger coloured symbols represent the average values for each meteorite. Error bars mark 1σ standard deviation from the mean.

primarily infilled voids left by brecciation (e.g. Fig. 8D) suggesting the early CO_2-rich and SO_2-rich fluids exploited the high permeability conduits. By contrast, the magnetite-carbonate clusters in the CY1s do not appear to have formed by precipitation into empty voids and open fractures but, instead, replaced former mineral phases. A third generation of carbonates can be inferred based on the presence of large (>100 μm) ferropericlase clasts (Fig. 5C and D) which are interpreted as former Fe-Mg-bearing carbonates (as explained in Section 4.4.2).

Accessory minerals provide further insights into the aqueous alteration history. In the CY2s phosphates occur as small grains with anhedral morphologies. Their outlines imply they previously existed as larger coherent phosphate clasts but suffered fluid attack and fracturing. Meanwhile, in the CY1s the phosphates are euhedral and co-occur with phyllosilicate and magnetite. A third variety of phosphate was recognised in Y-86789 (CY2). Here the phosphates are Mg-rich (Table 2) and occur within the fine-grained matrix infilling fractures, forming small-scale veins (Fig. S11). Thus, up to three generations of phosphate mineralisation can be recognised. During aqueous alteration P-bearing metal (schreibersite $(Fe, Ni)_3P$) would have been the main source of P. The anhedral vein deposits of Mg-apatite in Y-86789 are interpreted as the earliest generation to form and later suffered fluid attack and (incomplete) dissolution. The Ca-apatites found in B-7904 are likely to

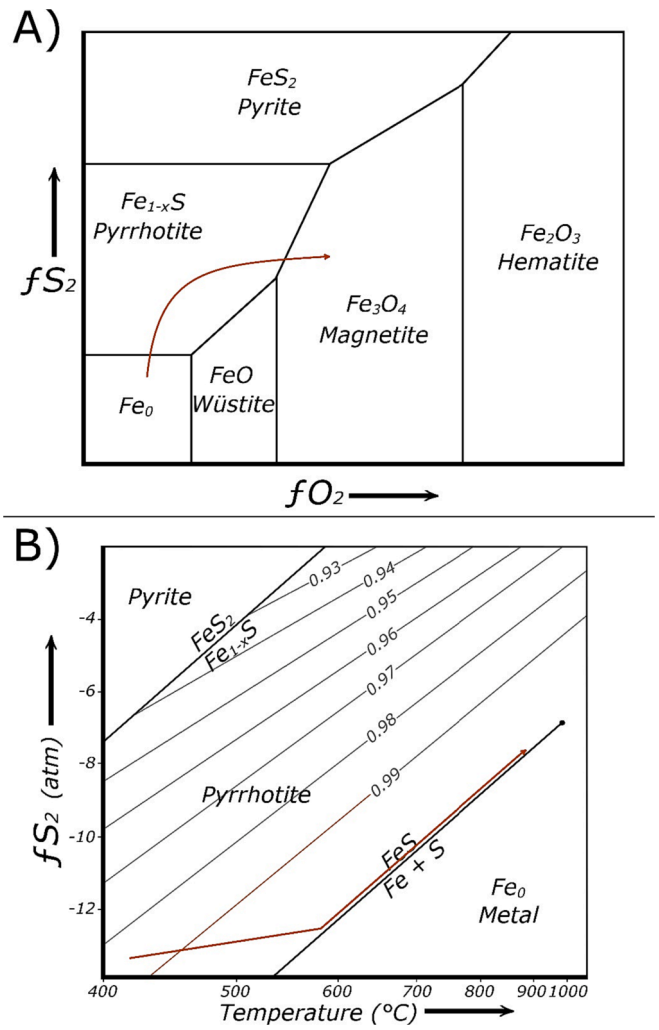

Fig. 11. Schematic sketches showing Fe-rich opaque mineral evolution (marked by red lines) during (A) aqueous alteration and (B) thermal metamorphism.

have been a second generation of phosphate growth and these were also affected by partial dissolution. Finally, the euhedral apatites in the CY1s, found in association with coarse phyllosilicates and magnetite would have been the last generation to form. Apatite in the CY chondrites has Cl-poor (<0.3 wt%) and F-poor (below detection limit) compositions, indicating low dissolved halogen abundances in the alteration fluids. Thus, the majority of the anion sites are occupied by OH- ions, producing compositions close to the hydroxylapatite end-member. Similar to those reported for other hydrated carbonaceous chondrites, including the CM chondrites, and C2-ungrouped materials (Piralla et al., 2021). By contrast, the CV and CK chondrites, non-carbonaceous chondrites and achondrites tend to have Cl-rich apatites (McCubbin et al., 2023). The halogen-poor apatites in hydrated chondrites appear to closely reflect the Solar System's initial Cl/F ratio and have been interpreted as evidence of closed-system alteration without external addition of F and Cl (Piralla et al., 2021).

Among the CY2s associations of Cr-spinel and ilmenite were identified. Textural and elemental analysis revealed two distinct generations of these refractory oxides. The initial generation are interpreted as having formed in the solar nebula prior to accretion. Conversely, the second generation of ilmenite and Cr-spinel grains precipitated during aqueous alteration, after the main window of phyllosilicate formation. This interpretation is based on the occurrence of Cr-spinel and ilmenite as deposits along the margins of coarse-grained phyllosilicates, found within altered chondrule cores (Fig. 1D). To a first order approximation, aqueous alteration in carbonaceous chondrites is the progressive conversion of amorphous and anhydrous silicates into phyllosilicates (McSween, 1979; Howard et al., 2009; Le Guillou et al., 2015; Suttle et al., 2021b). Alteration initially attacks the pre-hydrated amorphous silicates (King et al., 2021; Marrocchi et al., 2023) before altering the Fe-rich silicates and finally the Mg-rich silicates. Thus, over time progressively more Mg-rich silicates were dissolved, resulting in increasing Mg activities and the subsequent precipitation of more Mg-rich secondary phases (Velbel et al., 2015). The fraction of Mg present in the second generation of ilmenite and Cr-spinel is significantly higher than the corresponding primary oxides (Fig. 9). This observation is consistent with their formation from a Mg-bearing fluid phase and, therefore, late in the aqueous alteration sequence (after most Mg-bearing anhydrous silicates have been replaced).

In summary, the CY parent body experienced extensive alteration by evolving fluids in the C-H-O-N-P-S system. Early in the alteration sequence, metal was altered under low Si-activities and relatively high S-activities to Fe-sulphides (pyrrhotite). An initial generation of carbonates also formed concurrent with sulphide formation, infilling void spaces and hydrothermal fractures within the rock. An early Mg-apatite also formed at this stage within small-scale fractures in Y-86789. The intermediate stages of alteration were characterized by extensive silicate dissolution and the formation of phyllosilicates. This likely occurred at high water-to-rock (W/R) ratios, elevated temperatures, or elevated Si-activities leading to mixed serpentine/saponite assemblages and the formation of distinctive Na-saponite species. As these hydrated phases precipitated, they consumed water, increasing the activity of the remaining dissolved components, and increasing the likelihood of sulphide, carbonate, and phosphate formation. After phyllosilicate growth, and only within altered chondrules, refractory oxides (Cr-spinel and ilmenite) precipitated on the margins of phyllosilicates. During the later stages, as fS_2 decreased and fO_2 increased, some of the Fe-sulphide budget was reprocessed, becoming oxidized to form magnetite. At this time a second generation of carbonate co-precipitated with this magnetite. A third and final generation of large (>100 μm) Fe-Mg-bearing carbonates appear to have formed late in the alteration sequence.

4.4. Thermal metamorphic history and peak temperature estimates

In the CY chondrites thermal metamorphism overprinted aqueous alteration, as evidenced by the presence of dehydration cracks within the fine-grained matrix, their low bulk water contents (Lipschutz et al., 1999; King et al., 2015b) and the dehydrated, dehydroxylated and recrystallized phyllosilicates seen in XRD and TEM data (Akai, 1990; Nakamura, 2005; Nakato et al., 2008; King et al., 2019).

4.4.1. Closed system heating – evidence from sulphides

As temperature increased during metamorphic heating (arrowed path on Fig. 11B), pyrrhotite grains (FeS_{1+x}) would have progressively lost small amounts of sulphur (as S_2 gas), increasing the fS_2 (and aS_2) of the system and forming stoichiometric troilite (FeS) (Toulmin and Barton, 1964; Tomkins, 2009; Suttle et al., 2021a). Under further heating, small proportions of troilite thermally decompose to form Fe-metal + sulphur ($2FeS \rightarrow 2Fe + S_2$). If closed system conditions were maintained, then the liberated S_2 gas would have been unable to escape and the fS_2 of the system would increase along the troilite-metal buffer (Fig. 11B). Whilst held on this buffer, only a negligible quantity of troilite can decompose (note the log scale for $fS2$ on Fig. 11B), even if temperatures exceeded 900 °C. Thus, troilite can survive through peak metamorphic heating under these conditions. Later, during cooling any liberated S_2 would have back-reacted with metal, magnetite, and sulphides to form a new generation of troilite (Suttle et al., 2021a). By contrast, if heating occurred under open system conditions, the escape of S_2 gas would lead to the complete thermal decomposition of troilite (to metal) at relatively

modest temperatures (<680 °C). This is demonstrated by thermogravimetric analysis (TGA) experiments on Fe-sulphides heated in a through-flowing N_2 atmosphere, where removed S_2 gas from the system (e.g., Suttle et al., 2021a). Open system heating would also have left the CY assemblage dominated by metal instead of sulphide because the escaped S_2 was not available for back-reactions.

In the CY chondrites, some troilite grains contain small metal inclusions, typically taenite (Fig. 7). Their location along the perimeter or close to the outer margin of the grain supports their interpretation as evidence of inward troilite-to-metal decomposition (e.g., Kimura et al., 2011) and suggests that some Fe-sulphide was able to decompose and, therefore, that limited S_2 gas escape occurred. However, the widespread occurrence of troilite in the CYs is unambiguous evidence for near-closed system conditions during metamorphic heating. Furthermore, only a closed system scenario can explain both the observation of Fe-sulphides in the dehydration cracks in former phyllosilicates and the uniform composition of Fe-sulphides in all the CYs (Suttle et al., 2021a).

4.4.2. Carbonate decomposition

The CY2s contain a single generation of carbonates present as sulphide-carbonate clusters (as in Dho 1988, Fig. 8F), or their decomposition products (as in Y-86720, Fig. 8E). By contrast, in the CY1s two distinct carbonate generations can be identified. These occur as intact or partially decomposed sulphide-carbonate clusters (similar to those in the CY2s, e.g. Fig. 8D) and a second generation of magnetite-carbonate clusters (Fig. 8B and C). In addition, the CY1s also contain large (>100 μm scale) ferropericlase clasts containing inclusions of Fe-oxide and Fe-sulphide (Fig. 5C and D). Their chemical composition ([Fe,Mg]O) and presence of Fe-bearing inclusions suggest a formation mechanism by the thermal decomposition of complex (Fe-Mg-bearing) carbonates, as previously suggested by Tonui et al. (2003) and King et al (2019) and demonstrated experimentally by Jimenez-Lopez et al. (2012). Thus, the ferropericlase clusters most likely represent a third generation of carbonates that grew late in the aqueous alteration sequence and formed large sizes, growing from a fluid rich in dissolved Fe- and Mg- and, therefore, precipitating as carbonates with a mixed cation composition. This would explain why ferropericlase is not observed in the CY2s, only the CY1s. In addition, because increasing Fe content lowers the decomposition temperature of carbonate minerals (Tonui et al., 2003; Jimenez-Lopez et al., 2012), the formation of ferropericlase but retention of some intact or partially intact calcite/dolomite provides additional constraints on the peak metamorphic temperature experienced by the CY1s. Specifically, this differential preservation suggests peak temperatures >450 °C and <700 °C.

4.4.3. Thermal history as inferred from organic matter

In general, the Raman D and G bands of organic matter offer a chance to study the PMTs experienced by meteorites, as the structural transformation of the disordered or partly ordered, non-crystalline carbon-bearing material into crystalline graphite is an irreversible process, unless subsequently amorphized by other mechanisms such as space weathering (Beyssac et al., 2002). Typically, the process of graphitization is observable by the gradual change in the D band position and width, as the D band corresponds to the breathing modes in rings, which become observable when symmetry is broken by a crystallite edge (i.e., in-plane defects). Therefore, the D band is only present in organic matter with aromatic structure (Ferrari and Robertson, 2004) and, thus, serves as a strong tracer of the organic maturity. When subject to elevated temperature, the annealed organic matter will transform and become dominated by larger crystalline domains, which leads to a narrower D band width due to reduced defects, as illustrated by the trend of reducing ω_D and Γ_D values in chondrites with higher PMTs such as Allende (~600 °C) (Fig. 10A).

The G band corresponds to the C–C stretching vibration that traces graphitic ordering, as graphitic ordering reduces Γ_G. However, it has previously been observed that the Tagish Lake meteorite, which was exposed to short-term heating experiments (600° and 900 °C, for 1 and 96 h), showed significant widening of Γ_G, and the Γ_G value first increased and then decreased (Chan et al., 2019a). The organic material in the experimentally heated Tagish Lake samples significantly differs from that of chondritic organic matter modified by long-term internal heating. This trend runs counter to that observed for typical meteoritic organics, where decreasing Γ_G is associated with increasing metamorphism (e.g., Busemann et al., 2007; Bonal et al., 2016). A similar trend of wide Γ_G values has also been observed for interplanetary dust particles (IDPs) that have experienced short-term atmospheric entry heating, and that the Γ_G values of IDPs are at least ~18 cm^{-1} wider than those observed for chondritic material (Chan et al., 2019b). In this study, all CY group chondrites show a significant Γ_G widening by at least 11.2 cm^{-1} when compared to unheated chondritic organic matter (Fig. 10C and D). This observation suggests that the entire CY group has experienced short-term heating (or distinctive organic composition than other meteorite groups) and, therefore, the annealing of the organic components are influenced by both the temperature and duration of the heating.

We applied the model developed by Kiryu et al (2020) who considered the kinetics when using the Γ_D values, to estimate the time–temperature history of the CY group and its individual meteorites. However, in order to adopt this kinetic expression, either the duration or the temperature must be known, which is a chicken-and-egg scenario. Based on the estimations given by Nakamura (2005), that the temperatures corresponding to the heating stage are: Stage I (<300 °C); Stage II (300–500 °C); Stage III (500–750 °C); Stage IV (>750 °C), the PMTs of the two CY1s (Y-82162 spans 300–750 °C, Stage II-III and Y-86029 500–750 °C, Stage III) have lower peak temperatures than the four CY2 chondrites (B-7904, Y-86720 and Y86789 750–900 °C were all heated to Stage IV). These PMT estimations agree with the maturation hierarchy defined by the Γ_D parameter of Y-82162 (CY1) < Y-86029 (CY1) ≤ B-7904 (CY2) ≤ Y-86789 (CY2) ≤ Y-86720 (CY2). With these PMTs and using the model developed by Kiryu et al (2020), we estimate that the two CY1s (Y-82162 and Y-86029) were heated for ~3 h at 750 °C, or up to millions of years if heated at only 300 °C. Conversely, for the CY2s (B-7904, Y-86789 and Y-86720), the heating would be <1 day if the temperature was 750 °C. Or, at higher temperatures, up to ~900 °C, the heating duration would be as short as ~8 min. The precise heating scenario for the CYs most likely lies somewhere in between these ranges. Interestingly, these PMT estimates are consistent with the previous assessment by Nakato et al. (2008) based on the olivine cosmothermometer approach.

4.5. Origin and significance of high sulphide abundance in the CYs

The high Fe-sulphide abundance in the CY chondrites is one of the characteristic features that sets this group apart from the CM and CI chondrites. However, the origin and significance of this characteristic is unresolved. In Sect. 4.4.1., we argued that an initial generation of Fe-sulphides formed during fluid alteration, by sulphidation of metal and by direct precipitation. This interpretation has two important implications. Firstly, the CY parent body must have accreted abundant metal and, secondly, the fluids on the CY parent body were S-rich. To form S-rich fluids would require, either (1) the accretion of significant quantities of sulphur in a fluid-susceptible phase or, (2) the migration of evolved S-rich fluids from the deep interior of a complex and partially differentiated parent body into the undifferentiated primitive chondritic lid (e.g. Elkins-Tanton et al., 2011; Fu and Elkins-Tanton, 2014). These two options are considered further below:

(1) The fine-grained matrix in primitive chondrites contains amorphous material composed of Fe-Mg-silicates, which contains metal and sulphide inclusions. These phases are referred to as “GEMS-like” owing to their similarities with the “glass with embedded metal and sulphides” (GEMS) (Bradley, 1994) phases

found in cometary materials (Leroux et al., 2015; Le Guillou et al., 2015; Villalon et al., 2021). However, their S contents are relatively modest (at.% S/Si: <0.3) (Keller and Messenger, 2011; Leroux et al., 2015). Thus, unless the amorphous matrix material in the CY chondrites was atypically S-rich the accretion of this carrier phase could not account for the unique petrography of the CYs.

(2) Alternatively, if carbonaceous chondrites originate from the outer layers of an otherwise differentiated parent body, then the upwelling of evolved fluids (of magmatic or metamorphic origin) might explain the S-rich compositions of fluids in the CY chondrites. Elkins-Tanton et al. (2011) noted that the heating of chondritic materials in the interior to temperatures >430 °C would release sulphidic, and/or carbon-rich fluids that would rise efficiently into the chondritic crust. These fluids form by the dehydration of hydrated material held in the deep interior. Here, dehydration occurs because heat from radiogenic decay is retained more efficiently raising internal temperatures above the stability fields of the hydrated assemblage, leading to dehydration reactions and subsequent migration of fluids to lower density layers (e.g., Melwani Daswani et al., 2021). In such a scenario, the CY2 and CY1 petrologic grades reflect different environments within the chondritic crust, with fluid availability as the principal control on the extent of alteration. Thus, the spatial relationship between the CY2 and CY1 regions would depend on how the fluid migrated and accumulated within the crust. We note that one counter argument to the suggestion of aqueous alteration being driven by upwelling of evolved fluids with a magmatic or metamorphic origin is the inferred halogen-poor fluid compositions, based on the low abundances of Cl and F found in the precipitated apatite grains (Section 4.3 and Table 2).

Future isotopic studies analysing the composition of sulphides in CY chondrites may be able to resolve the origin of their anomalously high sulphide abundances.

4.6. Bulk O-isotopes and relationship of the CY chondrites to other chondrite groups

The CY chondrite group have a distinct ^{16}O-poor isotopic signature. This is heavier than all other carbonaceous chondrite groups (Fig. 12, approximately: $\delta^{17}O = 10.8$ ‰, $\delta^{18}O = 21.4$ ‰, $\Delta^{17}O = -0.3$ ‰, Clayton and Mayeda, 1999; King et al., 2019; Suttle et al., 2021a; Ito et al., 2022; Greenwood et al., 2023). Recently, Greenwood et al. (2023) studied the bulk compositions of two CYs (Y-82162 and B-7904) and noted that they have distinct $\Delta^{17}O$ values, despite similar $\delta^{18}O$ values. Their average $\Delta^{17}O$ compositions diverge by ~0.43 ‰ and on the basis of this observation Greenwood et al. (2023) suggested that the CY meteorites may not form a single homogeneous group. Likewise, Ito et al. (2022) reported a large intrasample variability ($\Delta^{17}O$ range of 0.18 ‰) based on seven measurements of Y-82162, reflecting small-scale isotopic heterogeneity within the CY lithology. This $\Delta^{17}O$ variability requires further investigation as several possible interpretations exist. The scale of variation could also mean that the CYs sample more than one closely related object (different parent bodies), or sample local-scale heterogeneity within a single parent body, potentially as a result of mass-dependent fractionation affecting specific mineral phases (e.g. Verdier-Paoletti et al., 2017). Finally, additional alteration arising due to terrestrial contamination could have further contaminated these Antarctic and hot-desert samples (Suttle et al., 2020; Greenwood et al., 2023).

In terms of the CYs relationship to other chondrite groups, they plot close to the CI chondrites and to the C2-ungrouped meteorites Tagish Lake and Tarda whilst overlapping with and extending above the Terrestrial Fractionation Line (TFL). The position of the CYs falls on a conceptual trendline, termed the "*CM mixing line*" (slope function of 0.7 and $\delta^{17}O$ intercept of −4.23 ‰; Rowe et al., 1994; Clayton and Mayeda, 1999). This trend is interpreted as isotopic exchange between two

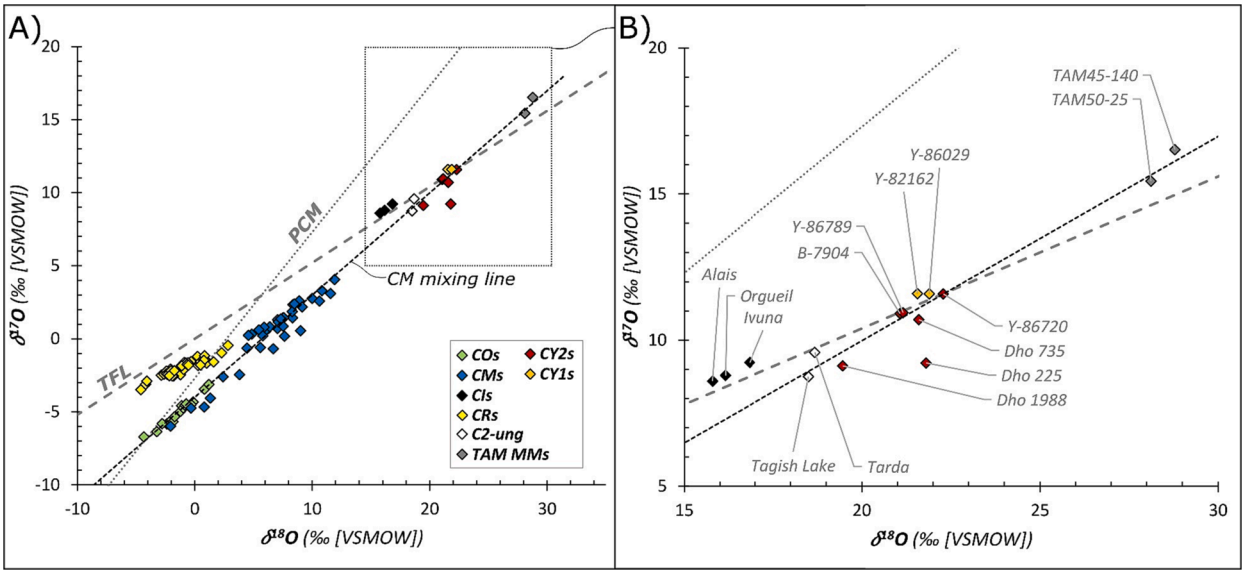

Fig. 12. The bulk O-isotope composition of the CY chondrites compared against the CO, CM and CI chondrites as well as the C2-ungrouped meteorites Tagish Lake and Tarda and a selected population of isotopically heavy ^{16}O-poor fine-grained unmelted micrometeorites. The dashed black box seen in panel A represented the magnified region shown in panel (B). (A) The CY chondrites have the heaviest reported composition of any chondrite group. (B) Their position in isotope space is close to (but distinct from) the CI chondrites. The CO, CM and CY chondrite groups (as well as the two micrometeorites) fall on the "*CM mixing line*" established by Clayton and Mayeda (1999). Also shown for reference are the terrestrial fractionation line (TFL, Lodders and Fegley, 1998) and the Primary Chondrule Mineral line (PCM) (Ushikubo et al., 2012). Data were taken from Clayton & Mayeda (1999), Brown et al. (2000); Moriarty et al. (2009), Ivanova et al. (2010), Schrader et al. (2011; 2014), Lee et al. (2016), Bouvier et al. (2017a; 2017b), Gattacceca et al. (2019), Lee et al. (2019), King et al. (2019) Kimura et al. (2020), Suttle et al. (2020; 2022b) and Greenwood et al. (2023).

primitive early solar system reservoirs, isotopically light anhydrous silicates and isotopically heavy water–ice grains (e.g., Clayton & Mayeda, 1984; 1999; Vacher et al., 2016, 2017; Verdier-Paoletti et al., 2017; Jilly-Rehak et al., 2018; Chaumard et al., 2018; Marrocchi et al., 2018; Suttle et al., 2020). The CM mixing line unites the bulk compositions of the CO and CM chondrites, and alongside other close petrographic and chemical similarities (Kallemeyn and Wasson, 1981; Schrader and Davidson, 2017; Alexander et al., 2018), is the basis for linking these two groups as the CO-CM chondrite clan (Weisberg et al., 2006). The position of the CY chondrites on the *CM mixing line* could reflect either:

(1) A close genetic link between the CY chondrites and the CO-CM chondrites, forming a larger CO-CM-CY clan. Considering trends between the CO and CM chondrites in terms of average chondrule size (~150 μm and ~300 μm, Weisberg et al., 2006) and chondrule abundance (~48 area% and ~20 area%, Weisberg et al., 2006) the CY chondrites appear to continue this trend, with fewer and larger chondrules (~320–340 μm and ~15 area%, Table 1). Meanwhile, the progressively heavier bulk O-isotope compositions may reflect accretion of proportionally more isotopically heavy water–ice onto the CY parent body than the CO and CM chondrites.
(2) Alternatively, the CYs may not be part of the CO-CM clan but, instead, coincidentally positioned on the *CM mixing line*. In this instance, the effects of mass-dependent fractionation on a former, lighter isotopic signature as a result of post-hydration thermal metamorphism could have played an important role in shifting the bulk CY chondrites to their current position (Valley, 1986; Clayton and Mayeda, 2009; Ivanova et al., 2013). In this scenario, the unheated (pre-metamorphic) position of the CY group would be approximately located on the TFL and potentially closer to the CI chondrite region than to the CM region.

To resolve these two possibilities requires further investigation of the CY chondrite isotopic signatures, which is beyond the scope of this study. Future work studying the isotopic composition of the chondrule silicates could reveal whether the CY chondrules originated from the same population as the CO and CM chondrules (e.g., Schrader and Davidson, 2017; Chaumard et al., 2018).

5. Implications

In this work we have shown that the six meteorites proposed as CY chondrites are united by similar accretionary properties and similar alteration histories. The CY chondrites span two petrologic grades (CY2 and CY1) with the CY1s recording more advanced aqueous alteration along approximately the same alteration sequence as the CY2s. Whether this grouping reflects a genetic relationship as fragments of the same first-generation parent body or whether the CY chondrites are merely a looser grouping of meteorites that formed on more than one closely related parent body remains unclear. Similar discussions exist for the CM chondrite group, asking whether the CMs originated from a single asteroid (e.g., Lee et al., 2019), reflecting the difficulty in reconstructing the early planestimals population. However, based on the observations in this work combined with the previous work of Ikeda (1992), King et al. (2019) and Suttle et al. (2021a), we propose the following criteria as diagnostic features of the CY chondrites:

Primary (accretionary) features

- Heavy O-isotope compositions ($\delta^{17}O$ = 10.8 ‰, $\delta^{18}O$ = 21.4 ‰, $\Delta^{17}O$ = −0.3 ‰ (Clayton and Mayeda, 1999; King et al., 2019).
- High metal abundances (which were later altered to form high Fe-sulphide abundances (10–30 vol%, King et al., 2019)).
- Low chondrule abundances (~15 area%) with apparent average diameters of approximately: 320–340 μm.
- High initial accreted water–ice abundances, similar to the water contents accreted by the CM and CI chondrites (high initial W/R mass ratios).

Secondary (alteration history) features

- An alteration history in which brecciation predates aqueous alteration and is later followed by short duration thermal metamorphism.
- A phyllosilicate-bearing matrix composed of both serpentine and saponite, including Na-saponite and low quantities of chlorite within altered chondrules.
- The occurrence of sulphide-carbonate assemblages precipitated within the fractures generated by early brecciation.
- The presence of halogen-poor hydroxylapatite and the co-occurrence of ilmenite and Cr-spinel as accessory minerals.
- Stochiometric low-Ni troilite as the dominant Fe-sulphide.
- The occurrence of large ferropericlase clasts (in the CY1s only), representing the thermal decomposition of large Fe-Mg-bearing carbonates.

6. Conclusions

We performed a detailed 2D petrographic investigation of six CY chondrite polished sections (four CY2s and 2 CY1s), analysing their mineralogy and petrology, and inferring their alteration history. The CYs record an early episode of brecciation, resulting in the formation of millimetre-sized clasts and a fragmented texture. Later, aqueous alteration precipitated secondary minerals within fractures and eroded the sharp compositional outlines between clasts. As in other carbonaceous chondrite groups, fluid-rock interactions replaced the accretionary mineralogy with hydrated phyllosilicates, Fe-sulphides (primarily pyrrhotite), carbonates and magnetite. Accessory minerals included Ca and Mg-bearing phosphates and refractory oxides (ilmenite and Cr-spinel). The extent of aqueous alteration was variable across the CY parent body, as evidenced by the presence of both partially altered CY2s and fully altered CY1s – in which chondrules do not survive. Comparison between mineral assemblages in the CY2s and CY1s demonstrates a transition towards more oxidizing and alkaline conditions. Aqueous alteration was later overprinted by thermal metamorphism. The partial decomposition of phyllosilicates and carbonates constrains peak temperatures to heating stages II-IV in the scheme of Nakamura (2005), approximately 750–900 °C. Our analysis of heated organic matter supports earlier suggestions that heating was short in duration (minutes to days in length) and, therefore, likely of impact origin.

Declaration of Competing Interest

The authors declare that they have no known competing financial interests or personal relationships that could have appeared to influence the work reported in this paper.

Data availability

The data underlying all figures in the main paper have been made available via deposition in an open-access online repository, accessible at: https://zenodo.org/record/8130734. This includes the geochemical data, BSE maps and EDX cation maps (Mg-Fe-Ca) as well as interpretive schematic sketches of each section and the Raman spectra.

Acknowledgements

We are grateful for the loan of Yamato Mountain polished meteorite sections provided by NIPR (No. 1794). AJK acknowledges funding through UKRI grant number MR/T020261/1. CH is funded by STFC grant number ST/V506904/1. We thank Maxime Piralla and two anonymous reviewers as well as the associate editor Yves Marrocchi for

their helpful suggestions and comments, which greatly improved this work.

Appendix A. Supplementary material

Supplementary tables (Table S1) and Figs. S1–S15 referred to in this article are provided as a single PDF file. This includes Raman data (Table S1) as well as high resolution BSE and EDS elemental maps for each section analysed (Figs. S1–S6), olivine chemical composition histograms for each section studied (Fig. S7), chondrule size distribution plots for the four CY2 meteorites (Fig. S8), BSE images of altered and pseudomorphic CAIs (Fig. S9), chemical compositions of Fe-metal and Fe-sulphide phases in each section studied (Fig. S10), BSE images of Mg-bearing apatite in Y-86789 (Fig. S11), chemical compositions of carbonate phases in the CY1s and CY2s (Fig. S12) and P-Ni-Ca-S EDX maps for three of the CY sections (Figs. S13–S15). Supplementary material to this article can be found online at https://doi.org/10.1016/j.gca.2023.09.024.

References

Abreu, N.M., Aponte, J.C., Cloutis, E.A., Nguyen, A.N., 2020. The Renazzo-like carbonaceous chondrites as resources to understand the origin, evolution, and exploration of the solar system. Geochem. 80, 125631.

Akai, J., 1990. Mineralogical evidence of heating events in Antarctic carbonaceous chondrites Y-86720 and Y-82162. Antarc. Met. Res. 3, 55–68.

Akai, J., 1992. T-T-T diagram of serpentine and saponite, and estimation of metamorphic heating degree of antarctic carbonaceous chondrites. Antarc. Met. Res. 5, 120–135.

Alexander, C.O.D., 2005. From supernovae to planets: the view from meteorites and interplanetary dust particles. In: Chondrites and the Protoplanetary Disk, ASP Conference Series, 341, pp. 972–1002.

Alexander, C.O.D., Bowden, R., Fogel, M.L., Howard, K.T., Herd, C.D.K., Nittler, L.R., 2012. The provenances of asteroids, and their contributions to the volatile inventories of the terrestrial planets. Science 337, 721–723.

Alexander, C.M.O'D., Greenwood, R.C., Bowden, R., Gibson, J.M., Howard, K.T., Franchi, I.A., 2018. A mutli-technique search for the most primitive CO chondrites. Geochim. Cosmochim. Acta 221, 406–420.

Alexander, C.M.D., Howard, K.T., Bowden, R., Fogel, M.L., 2013. The classification of CM and CR chondrites using bulk H, C and N abundances and isotopic compositions. Geochim. Cosmochim. Acta 123, 244–260.

Alfing, J., Patzek, M., Bischoff, A., 2019. Modal abundances of coarse-grained (>5 μm) components within CI-chondrites and their individual clasts–Mixing of various lithologies on the CI parent body (ies). Geochem 79, 125532.

Amsellem, E., Moynier, F., Mahan, B., Beck, P., 2020. Timing of thermal metamorphism in CM chondrites: Implications for Ryugu and Bennu future sample return. Icarus 339, 113593.

Bates, H.C., Donaldson Hanna, K.L., King, A.J., Bowles, N.E., Russell, S.S., 2021. A Spectral investigation of aqueously and thermally altered CM, CM-An, and CY chondrites under simulated asteroid conditions for comparison with OSIRIS-REx and Hayabusa2 observations. J. Geophys. Res. Planets 126.

Bates, H.C., King, A.J., Shirley, K.S., Bonsall, E., Schroeder, C., Wombacher, F., Fockenberg, T., Curtis, R.J., Bowles, N.E., 2023. The bulk mineralogy, elemental composition, and water content of the Winchcombe CM chondrite fall. Meteorit. Planet. Sci.

Beck, P., Maturilli, A., Garenne, A., Vernazza, P., Helbert, J., Quirico, E., Schmitt, B., 2018. What is controlling the reflectance spectra (0.35–150 μm) of hydrated (and dehydrated) carbonaceous chondrites? Icarus 313, 124–138.

Beyssac, O., Goffé, B., Chopin, C., Rouzaud, J.N., 2002. Raman spectra of carbonaceous material in metasediments: A new geothermometer. J. Metam. Geol. 20, 859–871.

Bischoff, A., Metzler, K., 1991. Mineralogy and petrography of the anomalous carbonaceous chondrites Yamato-86720, Yamato-82162, and Belgica-7904. Antarctic Mete. Res. 4, 226–246.

Bischoff, A., Palme, H., Ash, R.D., Clayton, R.N., Schultz, L., Herpers, U., Stöffler, D., Grady, M.M., Pillinger, C.T., Spettel, B., Weber, H., 1993. Paired Renazzo-type (CR) carbonaceous chondrites from the Sahara. Geochim. Cosmochim. Acta 57, 1587–1603.

Bischoff, A., Alexander, C.M.D., Barrat, J.A., Burkhardt, C., Busemann, H., Degering, D., Di Rocco, T., Fischer, M., Fockenberg, T., Foustoukos, D.I., Gattacceca, J., 2021. The old, unique C1 chondrite Flensburg-Insight into the first processes of aqueous alteration, brecciation, and the diversity of water-bearing parent bodies and lithologies. Geochim. Cosmochim. Acta 293, 142–186.

Bonal, L., Quirico, E., Bourot-Denise, M., Montagnac, G., 2006. Determination of the petrologic type of CV3 chondrites by Raman spectroscopy of included organic matter. Geochim. Cosmochim. Acta 70, 1849–1863.

Bonal, L., Quirico, E., Flandinet, L., Montagnac, G., 2016. Thermal history of type 3 chondrites from the Antarctic meteorite collection determined by Raman spectroscopy of their polyaromatic carbonaceous matter. Geochim. Cosmochim. Acta 189, 312–337.

Bouvier, A., Gattacceca, J., Agee, C., Grossman, J., Metzler, K., 2017a. The meteoritical bulletin, no. 104. Meteorit. Planet. Sci. 52, 2284.

Bouvier, A., Gattacceca, J., Grossman, J., Metzler, K., 2017b. The meteoritical bulletin, No. 105. Meteorit. Planet. Sci. 52, 2411.

Bradley, J.P., 1994. Chemically anomalous, pre-accretionally irradiated grains in interplanetary dust from comets. Science 265, 925–929.

Brearley, A.J., 1995. Aqueous alteration and brecciation in Bells, an unusual, saponite-bearing, CM chondrite. Geochim. Cosmochim. Acta 59, 2291–2317.

Brown, P.G., Hildebrand, A.R., Zolensky, M.E., Grady, M., Clayton, R.N., Mayeda, T.K., Tagliaferri, E., Spalding, R., MacRae, N.D., Hoffman, E.L., Mittlefehldt, D.W., 2000. The fall, recovery, orbit, and composition of the Tagish Lake meteorite: A new type of carbonaceous chondrite. Science 290, 320–325.

Bullock, E.S., Gounelle, M., Lauretta, D.S., Grady, M.M., Russell, S.S., 2005. Mineralogy and texture of Fe-Ni sulfides in CI1 chondrites: Clues to the extent of aqueous alteration on the CI1 parent body. Geochim. Cosmochim. Acta 69, 2687–2700.

Bunch, T.E., Chang, S., 1980. Carbonaceous chondrites—II. Carbonaceous chondrite phyllosilicates and light element geochemistry as indicators of parent body processes and surface conditions. Geochim. Cosmochim. Acta 44, 1543–1577.

Busemann, H., Alexander, M.O.D., Nittler, L.R., 2007. Characterization of insoluble organic matter in primitive meteorites by microRaman spectroscopy. Meteorit. Planet. Sci. 42, 1387–1416.

Chambers, J.E., 2004. Planetary accretion in the inner Solar System. Earth Planet. Sci. Lett. 223, 241–252.

Chan, Q.H.S., Zolensky, M.E., Bodnar, R.J., Farley, C., Cheung, J.C.H., 2017. Investigation of organo-carbonate associations in carbonaceous chondrites by Raman spectroscopy. Geochim. Cosmochim. Acta 201, 392–409.

Chan, Q.H.S., Nakato, A., Kebukawa, Y., Zolensky, M.E., Nakamura, T., Maisano, J.A., Colbert, M.W., Martinez, J.E., Kilcoyne, A.L.D., Suga, H., Takahashi, Y., Takeichi, Y., Mase, K., Wright, I.P., 2019a. Heating experiments of the Tagish Lake meteorite: Investigation of the effects of short-term heating on chondritic organics. Meteorit. Planet. Sci. 54, 104–125.

Chan, Q.H.S., Franchi, I.A., Zhao, X., Stephant, A., Wright, I.P., Alexander, C.M.O., 2019b. Organics preserved in anhydrous interplanetary dust particles: Pristine or not? Meteorit. Planet. Sci. 55, 1320–1348.

Chaumard, N., Defouilloy, C., Kita, N.T., 2018. Oxygen isotope systematics of chondrules in the Murchison CM2 chondrite and implications for the CO-CM relationship. Geochim. Cosmochim. Acta 228, 220–242.

Clayton, R.N., Mayeda, T.K., 1984. The oxygen isotope record in Murchison and other carbonaceous chondrites. Earth Planet. Sci. Lett. 67, 151–161.

Clayton, R.N., Mayeda, T.K., 1999. Oxygen isotope studies of carbonaceous chondrites. Geochim. Cosmochim. Acta 63, 2089–2104.

Clayton, R.N., Mayeda, T.K., 2009. Kinetic isotope effects in oxygen in the laboratory dehydration of magnesian minerals. Chem. A Eur. J. 113, 2212–2217.

Cody, G.D., Alexander, C.M.O'D., 2005. NMR studies of chemical structural variation of insoluble organic matter from different carbonaceous chondrite groups. Geochim. Cosmochim. Acta 69, 1085–1097.

Connolly Jr, H.C., Smith, C., Benedix, G., Folco, L., Righter, K., Zipfel, J., Yamaguchi, A., Aoudjehane, H.C., 2008. The Meteoritical Bulletin, No. 93. Meteorit Planet Sci. 43, 571–632.

Elkins-Tanton, L.T., Weiss, B.P., Zuber, M.T., 2011. Chondrites as samples of differentiated planetesimals. Earth Planet. Sci. Lett. 305, 1–10.

Feierberg, M.A., Lebofsky, L.A., Tholen, D.J., 1985. The nature of C-class asteroids from 3-μm spectrophotometry. Icarus 63, 183–191.

Ferrari, A.C., Robertson, J., 2000. Interpretation of Raman spectra of disordered and amorphous carbon. Phys. Rev. B 61, 14095.

Ferrari, A.C., Robertson, J., 2004. Raman spectroscopy of amorphous, nanostructured, diamond–like carbon, and nanodiamond. Philos. Trans. Royal Soc. A 362, 2477–2512.

Fries, M., Steele, A., 2011. Raman spectroscopy and confocal Raman imaging in mineralogy and petrography. In: Dieing, T., Hollricher, O., Toporski, J. (Eds.), Confocal Raman Microscopy. Springer, Berlin Heidelberg, pp. 111–135.

Fu, R.R., Elkins-Tanton, L.T., 2014. The fate of magmas in planetesimals and the retention of primitive chondritic crusts. Earth Planet. Sci. Lett. 390, 128–137.

Gattacceca, J., Bouvier, A., Grossman, J., Metzler, K., Uehara, M., 2019. The Meteoritical Bulletin, No. 106. Meteorit. Planet. Sci. 54, 469–471.

Greenwood, R.C., Franchi, I.A., Findlay, R., Malley, J.A., Ito, M., Yamaguchi, A., Kimura, M., Tomioka, N., Uesugi, M., Imae, N., Shirai, N., 2023. Oxygen isotope evidence from Ryugu samples for early water delivery to Earth by CI chondrites. Nat. Astron. 7, 29–38.

Guo, W., Eiler, J.M., 2007. Temperatures of aqueous alteration and evidence for methane generation on the parent bodies of the CM chondrites. Geochim. Cosmochim. Acta 71, 5565–5575.

Harju, E.R., Rubin, A.E., Ahn, I., Choi, B.G., Ziegler, K., Wasson, J.T., 2014. Progressive aqueous alteration of CR carbonaceous chondrites. Geochim. Cosmochim. Acta 139, 267–292.

Hezel, D.C., Russell, S.S., Ross, A.J., Kearsley, A.T., 2008. Modal abundances of CAIs: Implications for bulk chondrite element abundances and fractionations. Meteorit. Planet. Sci. 43, 1879–1894.

Howard, K.T., Benedix, G.K., Bland, P.A., Cressey, G., 2009. Modal mineralogy of CM2 chondrites by X-ray diffraction (PSD-XRD). Part 1: Total phyllosilicate abundance and the degree of aqueous alteration. Geochim. Cosmochim. Acta 73, 4576–4589.

Ikeda, Y., 1992. An overview of the research consortium, Antarctic carbonaceous chondrites with CI affinities, Yamato-86720, Yamato-82162, and Belgica-7904". Antarc. Met. Res. 5, 49–73.

Ito, M., Tomioka, N., Uesugi, M., Yamaguchi, A., Shirai, N., Ohigashi, T., Liu, M.C., Greenwood, R.C., Kimura, M., Imae, N., Uesugi, K., 2022. A pristine record of outer Solar System materials from asteroid Ryugu's returned sample. Nat. Astron 6, 1163–1171.

Ivanova, M.A., Lorenz, C.A., Nazarov, M.A., Brandstaetter, F., Franchi, I.A., Moroz, L.V., Clayton, R.N., Bychkov, A.Y., 2010. Dhofar 225 and Dhofar 735: Relationship to CM2 chondrites and metamorphosed carbonaceous chondrites, Belgica-7904 and Yamato-86720. Meteorit. Planet. Sci. 45, 1108–1123.
Ivanova, M.A., Lorenz, C.A., Franchi, I.A., Bychkov, A.Y., Post, J.E., 2013. Experimental simulation of oxygen isotopic exchange in olivine and implication for the formation of metamorphosed carbonaceous chondrites. Meteorit. Planet. Sci. 48, 2059–2070.
Jacquet, E., Piralla, M., Kersaho, P., Marrocchi, Y., 2021. Origin of isolated olivine grains in carbonaceous chondrites. Meteorit. Planet. Sci. 56, 13–33.
Jilly-Rehak, C.E., Huss, G.R., Nagashima, K., Schrader, D.L., 2018. Low-temperature aqueous alteration on the CR chondrite parent body: Implications from in situ oxygen-isotope analyses. Geochim. Cosmochim. Acta 222, 230–252.
Jimenez-Lopez, C., Rodriguez-Navarro, C., Rodriguez-Navarro, A., Perez-Gonzalez, T., Bazylinski, D.A., Lauer Jr, H.V., Romanek, C.S., 2012. Signatures in magnetites formed by (Ca, Mg, Fe)CO_3 thermal decomposition: Terrestrial and extraterrestrial implications. Geochim. Cosmochim. Acta 87, 69–80.
Kallemeyn, G.W., Wasson, J.T., 1981. The compositional classification of chondrites—I. The carbonaceous chondrite groups. Geochim. Cosmochim. Acta 45, 1217–1230.
Kebukawa, Y., Chan, Q.H., Tachibana, S., Kobayashi, K., Zolensky, M.E., 2017. One-pot synthesis of amino acid precursors with insoluble organic matter in planetesimals with aqueous activity. Sci. Adv. 3, e1602093.
Keller, L.P., Messenger, S., 2011. On the origins of GEMS grains. Geochim. Cosmochim. Acta 75, 5336–5365.
Kerridge, J.F., 1985. Carbon, hydrogen and nitrogen in carbonaceous chondrites: Abundances and isotopic compositions in bulk samples. Geochim. Cosmochim. Acta 49, 1707–1714.
Kikuchi, K., Nakamura, T., Nakashima, D., Nagao, K., Imae, N., Yamaguchi, A., Kojima, H., 2015. Yamato-980115: CI chondrite experienced incomplete dehydration deduced from mineralogy and noble gas signatures. 8th Kaikyokuiki Science Symposium.
Kikuchi, S., Shibuya, T., Abe, M., Uematsu, K., 2021. Experimental chondrite–water reactions under reducing and low-temperature hydrothermal conditions: Implications for incipient aqueous alteration in planetesimals. Geochim. Cosmochim. Acta 319, 151–167.
Kimura, M., Grossman, J.N., Weisberg, M.K., 2011. Fe-Ni metal and sulfide minerals in CM chondrites: An indicator for thermal history. Meteorit. Planet. Sci. 46, 431–442.
Kimura, M., Imae, N., Komatsu, M., Barrat, J.A., Greenwood, R.C., Yamaguchi, A., Noguchi, T., 2020. The most primitive CM chondrites, Asuka 12085, 12169, and 12236, of subtypes 3.0–2.8: Their characteristic features and classification. Polar Sci. 26, 100565.
King, A.J., Schofield, P.F., Howard, K.T., Russell, S.S., 2015a. Modal mineralogy of CI and CI-like chondrites by X-ray diffraction. Geochim. Cosmochim. Acta 165, 148–160.
King, A.J., Solomon, J.R., Schofield, P.F., Russell, S.S., 2015b. Characterising the CI and CI-like carbonaceous chondrites using thermogravimetric analysis and infrared spectroscopy. Earth Planets Space 67, 1–12.
King, A.J., Bates, H.C., Krietsch, D., Busemann, H., Clay, P.L., Schofield, P.F., Russell, S. S., 2019. The Yamato-type (CY) carbonaceous chondrite group: Analogues for the surface of asteroid Ryugu? Geochem 79, 125531.
King, A.J., Mason, E., Bates, H.C., Schofield, P.F., Donaldson Hanna, K.L., Bowles, N.E., Russell, S.S., 2021. Tracing the earliest stages of hydrothermal alteration on the CM chondrite parent body. Meteorit. Planet. Sci. 56, 1708–1728.
Kiryu, K., Kebukawa, Y., Igisu, M., Shibuya, T., Zolensky, M.E., Kobayashi, K., 2020. Kinetics in thermal evolution of Raman spectra of chondritic organic matter to evaluate thermal history of their parent bodies. Meteorit. Planet. Sci. 55, 1848–1864.
Kleine, T., Mezger, K., Palme, H., Scherer, E., Münker, C., 2005. Early core formation in asteroids and late accretion of chondrite parent bodies: Evidence from 182 Hf-182 W in CAIs, metal-rich chondrites, and iron meteorites. Geochim. Cosmochim. Acta 69, 5805–5818.
Kleine, T., Budde, G., Burkhardt, C., Kruijer, T.S., Worsham, E.A., Morbidelli, A., Nimmo, F., 2020. The non-carbonaceous–carbonaceous meteorite dichotomy. Space Sci. Rev. 216, 1–27.
Krot, A.N., Amelin, Y., Cassen, P., Meibom, A., 2005. Young chondrules in CB chondrites from a giant impact in the early Solar System. Nature 436, 989–992.
Krot, A.N., Nagashima, K., Alexander, C.M., Ciesla, F.J., Fujiya, W., Bonal, L., 2015. Sources of water and aqueous activity on the chondrite parent asteroids. In: Asteroids IV, pp. 635–660.
Lauretta, D.S., Buseck, P.R., Zega, T.J., 2001. Opaque minerals in the matrix of the Bishunpur (LL3. 1) chondrite: Constraints on the chondrule formation environment. Geochim. Cosmochim. Acta 65, 1337–1353.
Le Guillou, C., Changela, H.G., Brearley, A.J., 2015. Widespread oxidized and hydrated amorphous silicates in CR chondrites matrices: Implications for alteration conditions and H2 degassing of asteroids. Earth Planet. Sci. Lett. 420, 162–173.
Lee, M.R., Lindgren, P., King, A.J., Greenwood, R.C., Franchi, I.A., Sparkes, R., 2016. Elephant Moraine 96029, a very mildly aqueously altered and heated CM carbonaceous chondrite: Implications for the drivers of parent body processing. Geochim. Cosmochim. Acta 187, 237–259.
Lee, M.R., Cohen, B.E., King, A.J., Greenwood, R.C., 2019. The diversity of CM carbonaceous chondrite parent bodies explored using Lewis Cliff 85311. Geochim. Cosmochim. Acta 264, 224–244.
Lentfort, S., Bischoff, A., Ebert, S., Patzek, M., 2021. Classification of CM chondrite breccias—Implications for the evaluation of samples from the OSIRIS-REx and Hayabusa 2 missions. Meteorit. Planet. Sci. 56, 127–147.
Leroux, H., Cuvillier, P., Zanda, B., Hewins, R.H., 2015. GEMS-like material in the matrix of the Paris meteorite and the early stages of alteration of CM chondrites. Geochim. Cosmochim. Acta 170, 247–265.
Lipschutz, M.E., Zolensky, M.E., Bell, M.S., 1999. New petrographic and trace element data on thermally metamorphosed carbonaceous chondrites. Antarc. Met. Res. 12, 57–80.
Llovet, X., Moy, A.E., Pinard, P.T., Fournelle, J.H., 2021. Electron probe microanalysis: A review of recent developments and applications in materials science and engineering. Prog. Mater Sci. 116, 100673.
Lodders, K., Fegley, B., 1998. The Planetary Scientist's Companion. Oxford University Press on Demand.
Marrocchi, Y., Bekaert, D.V., Piani, L., 2018. Origin and abundance of water in carbonaceous asteroids. Earth Planet. Sci. Lett. 482, 23–32.
Marrocchi, Y., Libourel, G., 2013. Sulfur and sulfides in chondrules. Geochim. Cosmochim. Acta 119, 117–136.
Marrocchi, Y., Rigaudier, T., Piralla, M., Piani, L., 2023. Hydrogen isotopic evidence for nebular pre-hydration and the limited role of parent-body processes in CM chondrites. Earth Planet. Sci. Lett. 611, 118151.
Matsuoka, K., Nakamura, T., Nakamuta, Y., Takaoka, N., 1996. Yamato-86789: A heated CM-like carbonaceous chondrite. Antarc. Met. Res. 9, 20–36.
McCubbin, F.M., Lewis, J.A., Barnes, J.J., Boyce, J.W., Gross, J., McCanta, M.C., Srinivasan, P., Anzures, B.A., Lunning, N.G., Elardo, S.M., Keller, L.P., 2023. On the origin of fluorine-poor apatite in chondrite parent bodies. Am. Mineral. 108, 1185–1200.
McSween Jr, H.Y., 1979. Alteration in CM carbonaceous chondrites inferred from modal and chemical variations in matrix. Geochim. Cosmochim. Acta 43, 1761–1770.
Melwani Daswani, M., Vance, S.D., Mayne, M.J., Glein, C.R., 2021. A metamorphic origin for Europa's ocean. Geophys. Res. Lett. 48.
Moriarty, G.M., Rumble III, D., Friedrich, J.M., 2009. Compositions of four unusual CM or CM-related Antarctic chondrites. Geochem. 69, 161–168.
Nadoll, P., Angerer, T., Mauk, J.L., French, D., Walshe, J., 2014. The chemistry of hydrothermal magnetite. A review. Ore Geol. Rev. 61, 1–32.
Nakamura, T., 2005. Post-hydration thermal metamorphism of carbonaceous chondrites. J. Mineralog. Petrolog. Sci. 100, 260–272.
Nakamura, T., Nagao, K., Metzler, K., Takaoka, N., 1999. Heterogeneous distribution of solar and cosmogenic noble gases in CM chondrites and implications for the formation of CM parent bodies. Geochim. Cosmochim. Acta 63, 257–273.
Nakato, A., Nakamura, T., Kitajima, F., Noguchi, T., 2008. Evaluation of dehydration mechanism during heating of hydrous asteroids based on mineralogical and chemical analysis of naturally and experimentally heated CM chondrites. Earth Planet. Space 60, 855–864.
Ohnishi, I., Tomeoka, K., 2007. Hydrothermal alteration experiments of enstatite: implications for aqueous alteration of carbonaceous chondrites. Meteorit Planet Sci. 42, 49–61.
Palmer, E.E., Lauretta, D.S., 2011. Aqueous alteration of kamacite in CM chondrites. Meteorit. Planet. Sci. 46, 1587–1607.
Pignatelli, I., Marrocchi, Y., Vacher, L.G., Delon, R., Gounelle, M., 2016. Multiple precursors of secondary mineralogical assemblages in CM chondrites. Meteorit. Planet. Sci. 51, 785–805.
Pignatelli, I., Marrocchi, Y., Mugnaioli, E., Bourdelle, F., Gounelle, M., 2017. Mineralogical, crystallographic and redox features of the earliest stages of fluid alteration in CM chondrites. Geochim. Cosmochim. Acta 209, 106–122.
Pinto, G.A., Marrocchi, Y., Morbidelli, A., Charnoz, S., Varela, M.E., Soto, K., Martínez, R., Olivares, F., 2021. Constraints on planetesimal accretion inferred from particle-size distribution in CO chondrites. Astrophys. J. Lett. 917, L25.
Piralla, M., Tartese, R., Marrocchi, Y., Joy, K.H., 2021. Apatite halogen and hydrogen isotope constraints on the conditions of hydrothermal alteration in carbonaceous chondrites. Meteorit. Planet. Sci. 56, 809–828.
Pouchou, J.L., Pichoir, F., 1991. Quantitative analysis of homogeneous or stratified microvolumes applying the model "PAP". In: Heinrich, K.F.J., Newbury, D.E. (Eds.), Electron Probe Quantitation. Springer, New York, NY, pp. 31–75.
Rowe, M.W., Clayton, R.N., Mayeda, T.K., 1994. Oxygen isotopes in separated components of CI and CM meteorites. Geochim. Cosmochim. Acta 58, 5341–5347.
Rubin, A.E., Wasson, J.T., 1986. Chondrules in the Murray CM2 meteorite and compositional differences between CM-CO and ordinary chondrite chondrules. Geochim. Cosmochim. Acta 50, 307–315.
Russell, S.S., Suttle, M.D., King, A.J., 2022. Abundance and importance of petrological type 1 chondritic material. Meteorit. Planet. Sci. 57, 277–301.
Schindelin, J., Arganda-Carreras, I., Frise, E., Kaynig, V., Longair, M., Pietzsch, T., Preibisch, S., Rueden, C., Saalfeld, S., Schmid, B., Tinevez, J.Y., 2012. Fiji: an open-source platform for biological-image analysis. Nat. Methods 9, 676–682.
Schrader, D.L., Davidson, J., 2017. CM and CO chondrites: A common parent body or asteroidal neighbors? Insights from chondrule silicates. Geochim. Cosmochim. Acta 214, 157–171.
Schrader, D.L., Franchi, I.A., Connolly Jr, H.C., Greenwood, R.C., Lauretta, D.S., Gibson, J.M., 2011. The formation and alteration of the Renazzo-like carbonaceous chondrites I: Implications of bulk-oxygen isotopic composition. Geochim. Cosmochim. Acta 75, 308–325.
Schrader, D.L., Nagashima, K., Krot, A.N., Ogliore, R.C., Hellebrand, E., 2014. Variations in the O-isotope composition of gas during the formation of chondrules from the CR chondrites. Geochim. Cosmochim. Acta 132, 50–74.
Schrader, D.L., Davidson, J., McCoy, T.J., Zega, T.J., Russell, S.S., Domanik, K.J., King, A. J., 2021. The Fe/S ratio of pyrrhotite group sulfides in chondrites: An indicator of oxidation and implications for return samples from asteroids Ryugu and Bennu. Geochim. Cosmochim. Acta 303, 66–91.
Scott, E.R.D., Krot, A.N., 2003. Chondrites and their components. Treatise Geochem. 1 (711), 2–10.
Suttle, M.D., Dionnet, Z., Franchi, I., Folco, L., Gibson, J., Greenwood, R.C., Rotundi, A., King, A., Russell, S.S., 2020. Isotopic and textural analysis of giant unmelted

micrometeorites–identification of new material from intensely altered 16O-poor water-rich asteroids. Earth Planet. Sci. Lett. 546, 116444.
Suttle, M.D., Greshake, A., King, A.J., Schofield, P.F., Tomkins, A., Russell, S.S., 2021a. The alteration history of the CY chondrites, investigated through analysis of a new member: Dhofar 1988. Geochim. Cosmochim. Acta 295, 286–309.
Suttle, M.D., King, A.J., Schofield, P.F., Bates, H., Russell, S.S., 2021b. The aqueous alteration of CM chondrites, a review. Geochim. Cosmochim. Acta 299, 219–256.
Suttle, M.D., King, A.J., Ramkissoon, N.K., Bonato, E., Franchi, I.A., Malley, J., Schofield, P.F., Najorka, J., Salge, T., Russell, S.S., 2022a. Alteration conditions on the CM and CV parent bodies–Insights from hydrothermal experiments with the CO chondrite Kainsaz. Geochim. Cosmochim. Acta 318, 83–111.
Suttle, M.D., Folco, L., Dionnet, Z., Van Ginneken, M., Di Rocco, T., Pack, A., Scheel, M., Rotundi, A., 2022b. Isotopically heavy micrometeorites—Fragments of CY chondrite or a new hydrous parent body? J. Geophys. Res. 127.
Suttle, M.D., Daly, L., Jones, R.H., Jenkins, L., Van Ginneken, M., Mitchell, J.T., Bridges, J.C., Hicks, L.J., Johnson, D., Rollinson, G., Taylor, R., et al., 2023. The Winchcombe meteorite—A regolith breccia from a rubble pile CM chondrite asteroid. Meteorit. Planet. Sci.
Tomeoka, K., 1990. Mineralogy and petrology of Belgica-7904: A new kind of carbonaceous chondrite from Antarctica. Antarc. Met. Res. 3, 40–54.
Tomeoka, K., Buseck, P.R., 1988. Matrix mineralogy of the Orgueil CI carbonaceous chondrite. Geochim. Cosmochim. Acta 52, 1627–1640.
Tomeoka, K., Kojima, H., Yanai, K., 1989. Yamato-86720: A CM carbonaceous chondrite having experienced extensive aqueous alteration and thermal metamorphism. Antarc. Met. Res. 2, 55–74.
Tomkins, A.G., 2009. What metal-troilite textures can tell us about post-impact metamorphism in chondrite meteorites. Meteorit. Planet. Sci. 44, 1133–1149.
Tonui, E., Zolensky, M., Lipschutz, M., 2002. Petrography, mineralogy and trace element chemistry of Yamato-86029 Yamato-793321 and Lewis Cliff 85332: Aqueous alteration and heating events. Antarc. Met. Res. 15, 38–58.
Tonui, E.K., Zolensky, M.E., Lipschutz, M.E., Wang, M.-S., Nakamura, T., 2003. Yamato 86029: aqueously altered and thermally metamorphosed CI-like chondrite with unusual texture. Meteorit. Planet. Sci. 38, 269–292.
Toulmin, P.I., Barton, J., 1964. A thermodynamic study of pyrite and pyrrhotite. Geochim. Cosmochim. Acta 56, 227–243.
Tuinstra, F., Koenig, J.L., 1970. Raman spectrum of graphite. J. Chem. Phys. 53, 1126–1130.
Ushikubo, T., Kimura, M., Kita, N.T., Valley, J.W., 2012. Primordial oxygen isotope reservoirs of the solar nebula recorded in chondrules in Acfer 094 carbonaceous chondrite. Geochim. Cosmochim. Acta. 90, 242–264.
Vacher, L.G., Marrocchi, Y., Verdier-Paoletti, M.J., Villeneuve, J., Gounelle, M., 2016. Inward radial mixing of interstellar water ices in the solar protoplanetary disk. Astrophys. J. Lett. 827, L1.
Vacher, L.G., Marrocchi, Y., Villeneuve, J., Verdier-Paoletti, M.J., Gounelle, M., 2017. Petrographic and C & O isotopic characteristics of the earliest stages of aqueous alteration of CM chondrites. Geochim. Cosmochim. Acta 213, 271–290.
Vacher, L.G., Truche, L., Faure, F., Tissandier, L., Mosser-Ruck, R., Marrocchi, Y., 2019. Deciphering the conditions of tochilinite and cronstedtite formation in CM chondrites from low temperature hydrothermal experiments. Meteorit. Planet. Sci. 54, 1870–1889.
Vacher, L.G., Piani, L., Rigaudier, T., Thomassin, D., Florin, G., Piralla, M., Marrocchi, Y., 2020. Hydrogen in chondrites: Influence of parent body alteration and atmospheric contamination on primordial components. Geochim. Cosmochim. Acta 281, 53–66.
Valley, J.W., 1986. Stable isotope geochemistry of metamorphic rocks. Rev. min. Geochem. 16, 445–489.
Velbel, M.A., Tonui, E.K., Zolensky, M.E., 2015. Replacement of olivine by serpentine in the Queen Alexandra Range 93005 carbonaceous chondrite (CM2): Reactant–product compositional relations, and isovolumetric constraints on reaction stoichiometry and elemental mobility during aqueous alteration. Geochim. Cosmochim. Acta 148, 402–425.
Verdier-Paoletti, M.J., Marrocchi, Y., Avice, G., Roskosz, M., Gurenko, A., Gounelle, M., 2017. Oxygen isotope constraints on the alteration temperatures of CM chondrites. Earth Planet. Sci. Lett. 458, 273–281.
Villalon, K.L., Ohtaki, K.K., Bradley, J.P., Ishii, H.A., Davis, A.M., Stephan, T., 2021. Search for meteoritic GEMS II: Comparison of inclusions in amorphous silicates from the Paris chondrite and from anhydrous chondritic interplanetary dust particles. Geochim. Cosmochim. Acta 310, 346–362.
Warren, P.H., 2011. Stable-isotopic anomalies and the accretionary assemblage of the Earth and Mars: A subordinate role for carbonaceous chondrites. Earth Planet. Sci. Lett. 311, 93–100.
Weisberg, M.K., McCoy, T.J., Krot, A.N., 2006. Systematics and evaluation of meteorite classification. Meteorites and the early solar system II.
Wurm, G., Krauss, O., 2006. Concentration and sorting of chondrules and CAIs in the late solar nebula. Icarus 180, 487–495.
Yamaguchi, A., Tomioka, N., Ito, M., Shirai, N., Kimura, M., Greenwood, R.C., Liu, M.C., McCain, K.A., Matsuda, N., Uesugi, M., Imae, N., 2023. Insight into multi-step geological evolution of C-type asteroids from Ryugu particles. Nat. Astron 7, 398–405.
Zolotov, M.Y., 2012. Aqueous fluid composition in CI chondritic materials: Chemical equilibrium assessments in closed systems. Icarus 220, 713–729.